Power Electronics Research and Applications Transactions
https://www.sciltp.com/journals/perat

*Tutorial*

# Single-Inductor-Multiple-Output (SIMO) Inverters: Design and Applications

Albert Ting-Leung Lee [1,*,†] and Siew-Chong Tan (IEEE Fellow) [2,†]

[1] Department of Electrical and Computer Engineering, The University of Hong Kong, Hong Kong SAR, China
[2] Department of Electrical Engineering, The City University of Hong Kong, Hong Kong SAR, China
* Correspondence: tlalee@hku.hk
† These authors contributed equally to this work.

**How To Cite:** Lee, A.T.-L.; Tan, S.-C. Single-Inductor-Multiple-Output (SIMO) Inverters: Design and Applications. *Power Electronics Research and Applications Transactions* **2026**. https://doi.org/10.53941/perat.2026.100006

Received: 24 June 2026
Revised: 17 August 2026
Accepted: 20 August 2026
Published: 1 September 2026

**Abstract:** Single-inductor-multiple-output (SIMO) inverters offer a compact, proven and scalable solution for generating multiple AC or hybrid DC-AC outputs using a single magnetic component in the power stage. This approach enables lower cost, smaller form factor, reduced weight, and higher efficiency in low- to medium-power, space-constrained applications. This tutorial paper introduces the system architecture, circuit topologies and operating principles of baseline SIMO inverters. Advanced SIMO-derived architectures including SIMO AC-AC converters and bidirectional SIMO converters are also discussed. Key design considerations such as resonant tank design, main inductor selection and major power losses are addressed. In practice, SIMO inverters can act as multicoil wireless chargers in multicoil wireless power transfer (MC-WPT) systems.

**Keywords:** single-inductor multiple-output (SIMO); inverters; hybrid converters; multi-coil wireless power transfer (MC-WPT)

## 1. Introduction

A conventional approach to generate multiple independent DC supply voltages from a single DC voltage source is to use multiple DC-DC switching converters. Specifically, *N* single-output DC-DC switching converters are employed to produce *N* independent output voltages, which in turn requires *N* inductors. However, off-chip inductors are typically the bulkiest and heaviest components in a switch mode power supply (SMPS), making them difficult to integrate and miniaturize in DC-DC converter designs. To overcome this limitation, single-inductor multiple-output (SIMO) DC-DC converter, which uses only a single inductor in the power stage, have emerged as an attractive solution, which offers high compactness, reduced weight and lower cost [1–15]. These converters are widely used in power management ICs (PMICs) for system-on-chip (SoCs), microcontrollers (MCUs), and field programmable gate array (FPGAs), as well as in multistring LED drivers and battery-powered portable devices that require multiple supply rails.

Beyond DC-DC power conversion, the SIMO concept has also been extended to DC-AC power conversion. A new non-isolated DC-AC inverter topology, known as SIMO DC-AC boost inverter, was first introduced in [16,17]. Fundamentally, this inverter topology is formulated by appropriately integrating the functions of a conventional SIMO DC-DC converter with DC-AC resonant circuits. As a result, it can convert a single DC source into multiple independent sinusoidal-like AC outputs while requiring only one inductor in the power stage. Compared to traditional full-bridge inverters, this single-stage SIMO inverter is particularly advantageous for powering multiple transmitting coils in a multi-coil wireless power transfer (MC-WPT) system due to its simpler circuit structure, smaller size, lower cost, and greater flexibility and scalability.

Similar to its DC-DC counterpart, the SIMO inverter can be realized in buck-only, boost-only, or buck-boost configurations. In particular, a novel inverting buck-boost SIMO inverter was subsequently introduced in [18].

This topology enables single-stage DC-AC conversion from a single DC power source into multiple independent AC output voltages, with RMS values that can be either higher or lower than the input DC voltage. Besides, the SIMO inverter can operate in pseudo-continuous conduction mode (PCCM), where a higher average inductor current enables increased output power.

To further broaden the scope of the SIMO concept, its capability to simultaneously perform both DC-DC and DC-AC power conversions has also been explored. In [19], a SIMO DC-AC/DC hybrid converter capable of generating multiple AC and DC outputs was proposed. Indeed, this topology constitutes a significant improvement over conventional hybrid converters, including single-stage and two-stage boost-derived hybrid converters (BDHCs) [20,21], modified BDHCs [22–24], and quadratic BDHCs [25]. In particular, the proposed SIMO hybrid converter exhibits much lower circuit complexity for AC power generation, since only one additional power switch is required for each AC output channel, whereas conventional hybrid converters generally require a dedicated four-switch H-bridge inverter for every AC output. Consequently, the SIMO-based hybrid converter provides a smaller, cost-effective and scalable solution, especially in applications involving multiple AC outputs. Furthermore, unlike traditional hybrid converters, which are typically limited to a single DC output, the proposed topology is capable of supplying multiple DC outputs. It can also be configured for standalone AC-only or DC-only operation. These advantages make it well suited for applications that require simultaneous AC and DC power delivery from a single DC source, such as hybrid chargers or power banks with a Qi wireless charging pad and multiple USB charging ports.

Recently, a new family of SIMO AC-AC converters was proposed in [26–29]. These converters employ only a single inductor in the power stage and an appropriate switching sequence to achieve single-stage power conversion from an AC power source to multiple independent AC output voltages, without the need for an intermediate DC link. This simplifies the overall power conversion process and reduces energy losses associated with multi-stage conversion. Moreover, the absence of a bulky DC-link capacitor and the use of fewer components enable a more compact converter design, which is especially beneficial in space-constrained applications. In practice, they can act as compact, low-cost, and efficient multi-coil wireless chargers powered directly from a universal AC mains supply, avoiding the need for an additional AC-DC adapter and improving system integration. In [29], a non-isolated buck-boost hybrid converter with AC-AC/DC power conversion is introduced, enabling simultaneous wired and wireless power transfer.

In emerging applications such as actuation and energy harvesting of ultrasonic motors (USMs), vehicle-to-grid (V2G) for electric vehicles, peer-to-peer wireless power transfer (P2P-WPT) between mobile devices, individual ports may dynamically operate either as energy sources or loads depending on their state of charge, power demand and operating conditions. This creates a strong demand for peer-to-peer charging capability, where energy can be directly transferred from one storage unit to another without relying exclusively on a centralized power source. Such functionality is particularly attractive for improving energy availability, enhancing system resilience, enabling cooperative charging, and maximizing the utilization of distributed energy resources. Under these conditions, bidirectional power flow becomes essential for supporting energy redistribution, battery equalization, regenerative energy recovery, and source-load coordination. Motivated by the growing need for compact, efficient and flexible multiport power conversion interfaces capable of supporting peer-to-peer (P2P) energy exchange, a new family of bidirectional SIMO converters has been developed in [30–33]. Compared with conventional solutions based on multiple discrete unidirectional converters, a bidirectional SIMO topology can reduce component count, converter volume and system cost while improving integration and power density. In addition, by consolidating multiple power paths within a unified conversion structure, bidirectional SIMO converters offer enhanced control flexibility and scalability, and more effective energy management among interconnected ports. Hence, they provide a promising enabling technology for next-generation P2P charging systems requiring high efficiency, multifunctionality, compactness and flexible power sharing.

The paper is organized as follows. Section II introduces the system architecture of a baseline SIMO inverter. Section III presents the circuit topology, operating principle of the boost-only SIMO inverter. Section IV describes the circuit topology and operating principle of the inverting buck-boost SIMO inverter. Section V presents the circuit topology and operating principle of the SIMO DC-AC/DC hybrid converter. Section VI introduces advanced SIMO topologies such as SIMO AC-AC converters and bidirectional SIMO converters. Section VII discusses practical design considerations. Finally, Section VIII draws the conclusions of the paper.

## 2. System Architecture

The main functional block of a SIMO DC–AC converter, also known as a SIMO inverter, integrates a conventional SIMO DC–DC converter with a DC–AC stage comprising multiple resonant tanks connected in parallel. This architecture achieves single-stage DC-AC power conversion, enabling a single controller to simultaneously regulate all AC output voltages. Figure 1 shows the system architecture of the SIMO inverter.

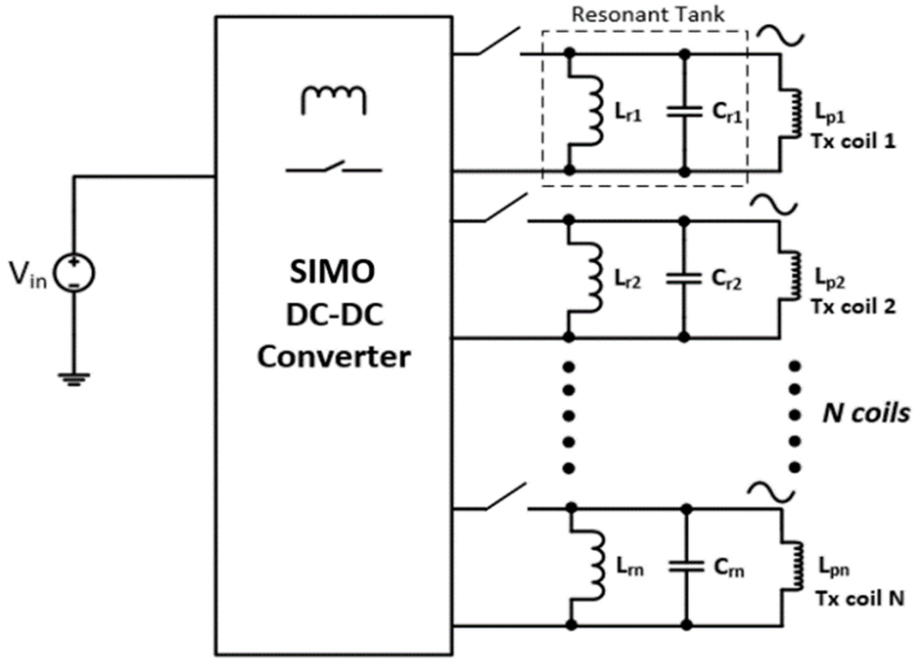


**Figure 1.** System architecture of a single-stage SIMO inverter.

The DC voltage source is converted into pulsed current by the main inductor, whose stored energy is subsequently delivered to each resonant tank sequentially in a round-robin, time-multiplexed manner. Each resonant tank, which may be implemented as a parallel combination of a resonant inductor and capacitor, converts the DC current pulse into an AC power source operating at the resonant frequency. These AC power sources then drive their respective output loads. The loads are controlled independently and are fully decoupled from one another, with no cross-interference. The output power of each channel is regulated individually by adjusting the corresponding on-time duty ratio of the main power switch. The proposed SIMO topology operating in discontinuous conduction mode (DCM) is particularly suitable for low-power wireless power transfer applications.

The main inductor $L$ acts as a current source, sequentially delivering its stored energy to each AC output. In theory, the maximum deliverable output power is limited by the energy stored in $L$, which is determined by its inductance and maximum current rating. Since the power stage employs only a single inductor, the maximum power available to each output is relatively limited. Moreover, because this SIMO topology operates in DCM, it is best suited for light-load conditions, where higher efficiency can be achieved through reduced conduction losses and zero-current switching (ZCS). Therefore, in practical applications, the proposed topology can be used as a low-power multichannel wireless transmitter for concurrently charging multiple mobile devices.

In wireless power transfer applications, the load is typically the inductive transmitter coil. Energy is delivered from the transmitter coil to the receiver coil of a compatible device placed in proximity via magnetic coupling. Since the resonant inductor is connected in parallel with the transmitter coil, as shown in Figure 1, its inductance should therefore be much smaller than that of the transmitter coil. This helps ensure that the resonant frequency is not substantially affected when the transmitter coil is loaded.

The SIMO inverter can be configured as boost-only, inverting or non-inverting buck-boost type. The circuit topology and operating principle of each type will be elucidated in detail in the following section.

## 3. Boost SIMO Inverter

### *3.1. Circuit Topology*

In principle, the non-isolated boost SIMO inverter topology is derived by integrating the functions of a traditional DC-DC boost converter (Figure 2a) and a parallel network of LC resonant tanks loaded by the respective inductive coil (Figure 2b) into a single-stage inverter (Figure 2c) [6].

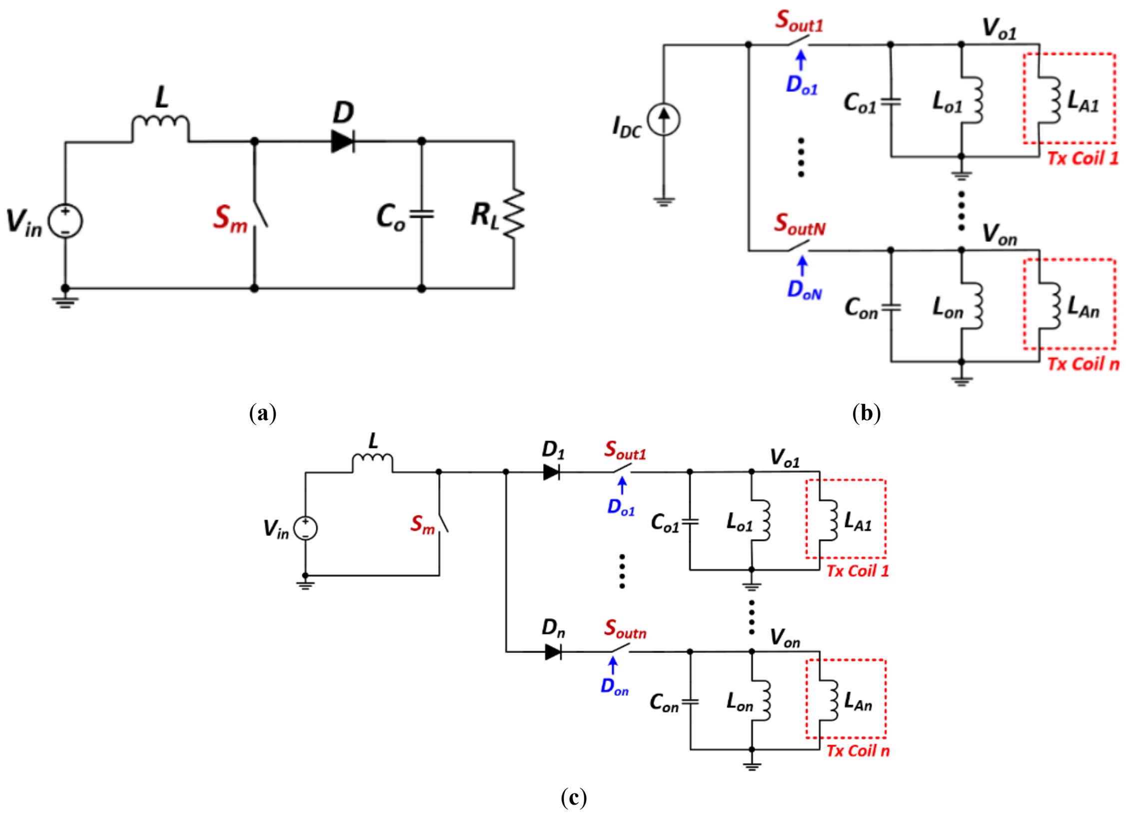


**Figure 2.** (**a**) Conventional DC-DC boost converter; (**b**) parallel network of LC resonant tanks; and (**c**) circuit topology of SIMO boost inverter.

In this configuration, the main inductor $L$ of the DC-DC boost converter in Figure 2a serves as a current source, replacing the independent current source ($I_{DC}$) and delivering the stored energy successively to each individual AC output in a time-multiplexed, round-robin manner. When the LC resonant tank is excited at its resonant frequency, it oscillates and generates the corresponding AC output voltage or current. Since the boost converter and the resonant tanks share a common ground, the two circuits can be naturally and conveniently combined to form a single-stage single-inductor multiple-output inverter. For the same number of AC outputs, the proposed SIMO inverter is superior to conventional inverters such as full-bridge inverters [34–38] because it requires fewer power switches, gate drivers and passive components in attaining robust DC-AC power conversion. No isolated transformer is used in the proposed inverter, which significantly reduces the overall form factor and weight, and increases the power density. Without loss of generality, the following analysis considers a single-inductor three-output (SITO) boost inverter, whose circuit topology is depicted in Figure 3.

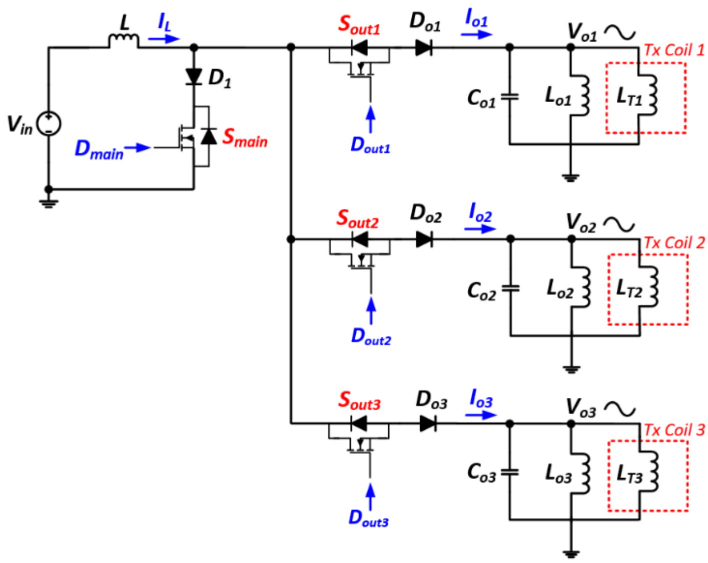


**Figure 3.** Ideal circuit diagram of single-inductor three-output (SITO) boost-only inverter.

This inverter transforms a single DC input voltage ($V_{in}$) into three independent AC output voltages ($V_{o1}$, $V_{o2}$, $V_{o3}$). A total of four switches are used, including one main switch ($S_{main}$) and three switches ($S_{out1}$, $S_{out2}$, $S_{out3}$). Each switch is implemented using a silicon power MOSFET. The gate-drive signals for the corresponding MOSFETs are represented as $D_{main}$, $D_{o1}$, $D_{o2}$ and $D_{o3}$, respectively. Only one main inductor $L$ is used in the power stage, and the current across $L$ is denoted as $I_L$. Each output branch comprises a parallel LC resonant tank, namely, ($L_{o1}$, $C_{o1}$), ($L_{o2}$, $C_{o2}$), and ($L_{o3}$, $C_{o3}$), which is connected to the corresponding load ($L_{T1}$, $L_{T2}$, $L_{T3}$). Anti-series blocking diodes are also employed. Specifically, diode $D_1$ prevents unintended reverse current from flowing from ground to the negative output through the internal body diode of $S_{main}$ during the second subinterval of DCM, i.e., the discharging phase, when $S_{main}$ is turned OFF and the corresponding output switch is turned ON. Likewise, the output diode ($D_{o1}$) prevents undesirable reverse current from flowing from the first AC output to the DC input through the internal body diode of $S_{out1}$ when the instantaneous output voltage exceeds the DC input voltage. Basically, the internal body diode of $S_{out1}$ and the blocking diode ($D_{o1}$) are connected in series but pointing in opposite direction, hence forming an effective back-to-back diode structure to ensure unidirectional current flow from the main inductor to the first output. The same configuration is used for the other two outputs.

### *3.2. Operating Principle*

For ease of understanding, the power stage of the SITO boost inverter is represented by a simplified equivalent circuit employing ideal switches, with the anti-series diodes omitted. In the equivalent circuit, the ON/OFF status of each switch alongside the direction of the main inductor current are indicated. The illustration shown here corresponds to the general case of unbalanced load, in which the inverter drives different AC loads at its outputs. By default, each switching state is uniquely represented as ($x$, $y$), where $x$ is the output number and $y$ is the mode of operation. For instance, state (1-1) refers to the first output and Mode 1. Figure 4a shows the switching states and operating sequence of this inverter. Figure 4b shows the theoretical waveforms of the gate-drive signals of main switch ($D_{main}$) and output switches ($D_{out1}$, $D_{out2}$, $D_{out3}$), inductor current ($I_L$), output branch currents ($I_{o1}$, $I_{o2}$, $I_{o3}$), and the three AC output voltages ($V_{o1}$, $V_{o2}$, $V_{o3}$). The SITO inverter operates in DCM at a fixed switching frequency ($f_s$), where $f_s = \frac{1}{T_s}$, and $T_s$ is the switching period. Under DCM operation, each output occupies one full switching period, during which the inverter undergoes three distinct operating modes. As a result, there are *nine* independent states in total, as depicted in Figure 4a. The on-time duty ratios of $S_{main}$ corresponding to the first, second and third output are denoted by $D_{11}$, $D_{21}$, and $D_{31}$, respectively. Under unbalanced load conditions, different power levels are delivered to the three outputs. Figure 4b illustrates one such condition, where $D_{11} < D_{21} < D_{31}$. Hence, the inductor current $I_L$ exhibits *different* peak values for the three outputs, namely $I_{L,pk1} < I_{L,pk2} < I_{L,pk3}$, where $I_{L,pk1}$, $I_{L,pk2}$ and $I_{L,pk3}$ represent the peak values of $I_L$ for the first, second and third outputs, respectively. Without loss of generality, the operating principle of the SITO inverter is explained using the *first* output since the operating modes are identical for all outputs.

In state (1-1) shown in Figure 4a, the inverter operates in the first subinterval of DCM (Mode 1). $S_{main}$ is switched ON while all output switches are OFF. This corresponds to Mode 1 in DCM operation during which the main inductor $L$ is charged up. $I_L$ increases with a positive slope of $m_{11}$, where $m_{11} = V_{in}/L$, until it reaches the peak value of $I_{L,pk1}$, which can be expressed as

$$I_{L,pk1} = m_{11} D_{11} T_s = \left(\frac{V_{in}}{L}\right) D_{11} T_s \tag{1}$$

where $V_{in}$ is the input voltage, $D_{11}$ is the on-time duty ratio for the first output, and $T_s$ is the switching period. It should be noted that $m_{11}$ is independent of the output voltage and hence, its value is the same across all outputs, i.e., $m_{11} = m_{21} = m_{31} = V_{in}/L$.

In state (1-2), the inverter operates in the second subinterval of DCM (Mode 2). $S_{main}$ is switched OFF and $S_{out1}$ is switched ON. The energy stored in $L$ is transferred to the first AC output. $I_L$ decreases with a negative slope of $m_{12}(t)$, which is given by

$$m_{12}(t) = \frac{\left[V_{in} - V_{o1}(t)\right]}{L} \tag{2}$$

where $V_{o1}(t)$ is the sinusoidal voltage of the first output.

Since $V_{o1}(t)$ is a time-varying sinusoidal waveform, whereas $V_{in}$ is a constant DC voltage, $m_{12}(t)$ varies nonlinearly and exhibits a convex downward profile. As a first-order approximation, the variation of $V_{o1}(t)$ over the short duration of Mode 2 is sufficiently small to be neglected. Therefore, $V_{o1}(t)$ can be approximated by its average value during Mode 2, which is given by

https://doi.org/10.53941/perat.2026.100006

$$m_{12}(t) = \frac{V_{in} - \overline{V_{o1,m12}}}{L} \quad (3)$$

where $\overline{V_{o1,m12}}$ denotes the average value of the first output voltage in Mode 2. Eventually, $L$ is fully discharged and $S_{o1}$ is switched OFF at the zero-crossing of $I_L$.

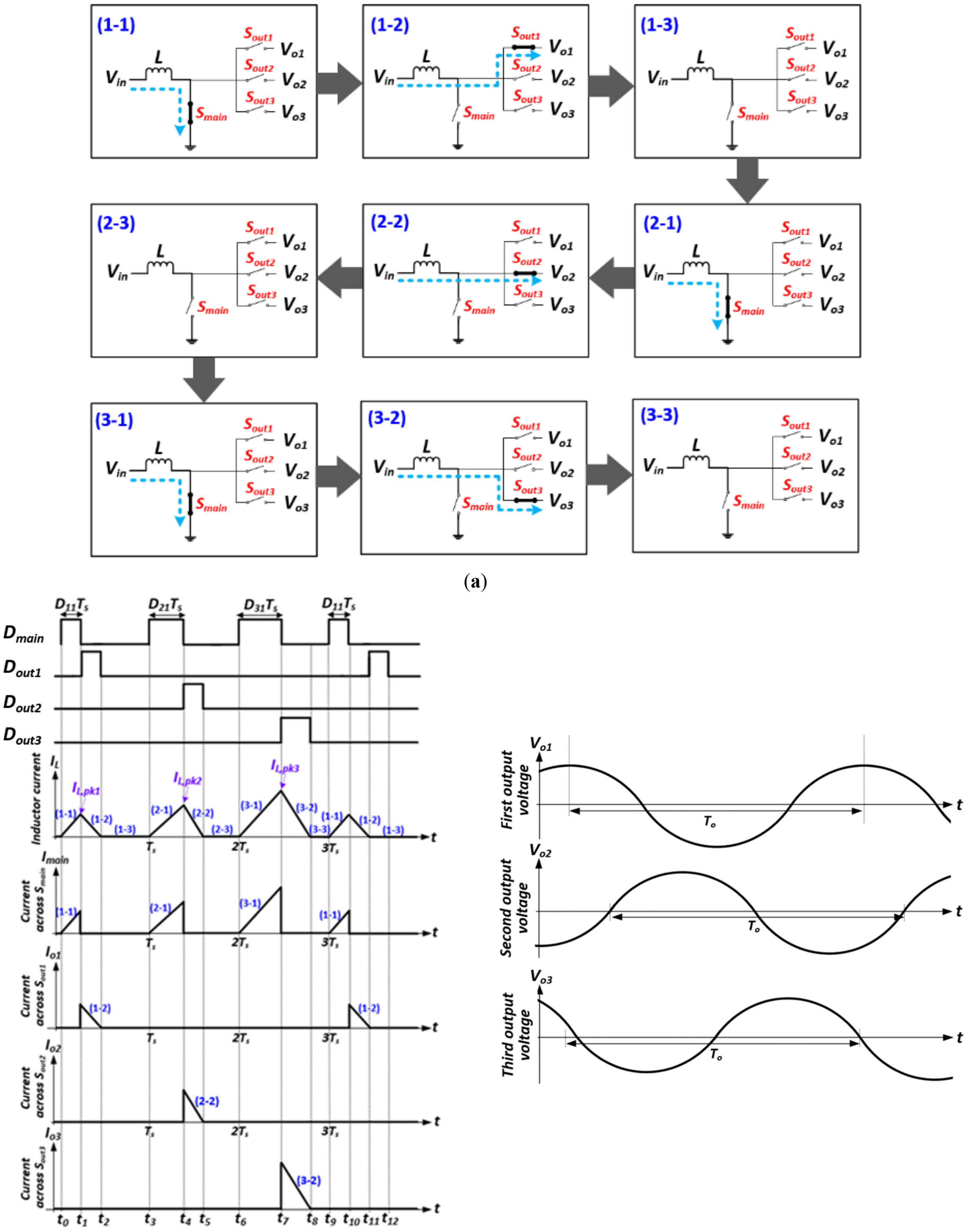


(a)

(b)

**Figure 4.** (**a**) Switching states and operating sequence of the boost SITO inverter; (**b**) theoretical waveforms of the gate-drive signals for the main switch, output switches, main inductor current, output branch currents, and three AC output voltages.

In state (1-3), the inverter operates in the third subinterval of DCM (Mode 3). All switches are OFF, and $I_L$ remains at zero value. This idle interval is essential for preventing unwanted cross-regulation among the outputs. The end of state (1-3) marks the completion of the switching cycle for the first output and the start of the switching cycle for the second output. The same sequence of mode transitions then occurs for the second output, followed by the third output. At the end of state (3-3), the SITO inverter completes one full resonant period ($T_o$), where $T_o = 3T_s$. In other words, the switching frequency of $S_{main}$ ($f_s$) of the inverter is three times the resonant frequency of the LC resonant tank. Mathematically, it can be expressed as

$$f_s = 3f_o = \frac{3}{2\pi\sqrt{L_o C_o}} \quad (4)$$

where $L_o$ and $C_o$ are the resonant inductor and resonant capacitor, respectively.

## 4. Buck-Boost SIMO Inverter

The aforementioned boost SIMO inverter has two major drawbacks. First, it delivers only modest output power, which is insufficient to meet the increasing power demands of portable electronic devices. Second, the RMS value of the sinusoidal output voltage must exceed the DC value of the input voltage, unnecessarily constraining the voltage requirements of the load devices. To overcome such limitations, a novel buck-boost SIMO inverter is introduced in [8]. By operating in pseudo-continuous conduction mode (PCCM), a higher output power can be achieved. Also, it is capable of producing multiple independent AC output voltages whose RMS values can be higher or lower than the DC input voltage.

### *4.1. Circuit Topology*

Fundamentally, this inverter topology is formulated by integrating the functions of an inverting buck-boost DC-DC converter and an independent DC current source supplying a parallel network of LC resonant tanks, as shown in Figure 5.

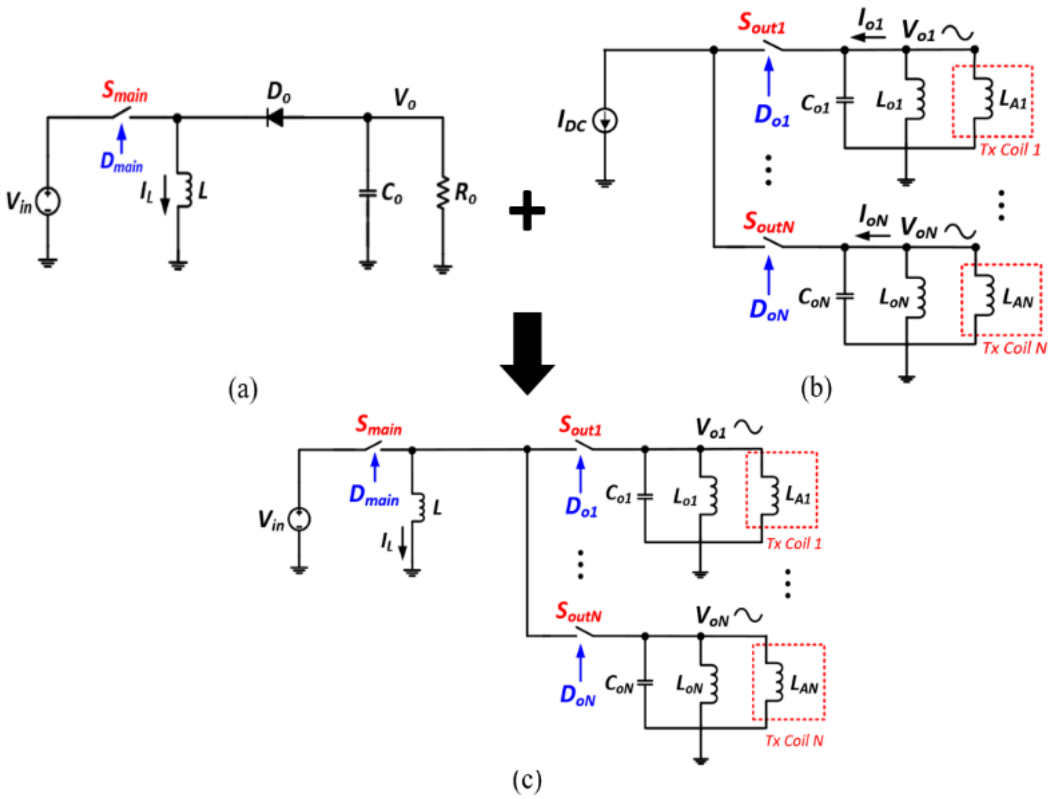


**Figure 5.** (**a**) Inverting buck-boost DC-DC converter; (**b**) a current source supplying a parallel network for LC resonant tanks; and (**c**) single-stage buck-boost DC-AC SIMO inverter.

It should be noted that the inverting buck-boost DC-DC converter produces a negative DC output voltage. However, the output polarity for the inverting buck-boost DC-AC SIMO inverter is inconsequential because the outputs are sinusoidal. The only effect of the reversed polarity is a 180° phase shift in the sinusoidal output voltage, which does not affect the inverter's functionality in any way. Practically speaking, the inverting buck-boost inverter topology is preferred to its non-inverting counterpart since the former requires fewer power switches and gate drivers, resulting in smaller component count, lower cost, and higher efficiency.

Figure 6 shows the circuit topology of an inverting buck-boost single-inductor three-output (SITO) inverter. For simplicity, an ideal circuit is assumed, and non-idealities such as the equivalent series resistance (ESR) of the capacitors and the DC resistance (DCR) of the inductors are neglected. The SITO inverter converts a single DC input voltage ($V_{in}$) into three independent AC output voltages ($V_{o1}$, $V_{o2}$, $V_{o3}$). However, unlike its predecessor [6], the RMS value of each output voltage can be adjusted to be either higher or lower than $V_{in}$ by controlling the corresponding on-time duty cycle of $S_{main}$. To reduce conduction loss, a pair of back-to-back freewheeling switches is used instead of an anti-series diode connected in series with the power MOSFET. The pair of back-to-back switches also prevents unintended conduction through the MOSFET body diode when the device is switched OFF. As a result, the inverter requires a total of nine power MOSFETs: one for the main switch and two for each output switch.

To enable PCCM operation, a pair of freewheeling MOSFETs is connected across the main inductor $L$. It is worth noting that back-to-back freewheeling switches is used to eliminate a direct short circuit between the switching node $V_s$ and ground via the body diode of the freewheeling switch. Suppose only one freewheeling switch is connected across $L$, that is, the upper freewheeling switch $S_{1,fw}$ is removed and only the lower switch $S_{2,fw}$ remains. When $S_{out1}$ is turned ON and the sinusoidal output voltage $V_{o1}$ becomes negative during the second subinterval of PCCM (or DCM), $V_s$ also becomes negative. This, in turn, creates an undesired reverse current path from ground to $V_s$ through the body diode of $S_{2,fw}$, even though the switch itself is turned OFF. Clearly, this is not the intended operating behavior. Therefore, two back-to-back freewheeling MOSFETs, with their body diodes oriented in opposite directions, are essential in the proposed SITO inverter.

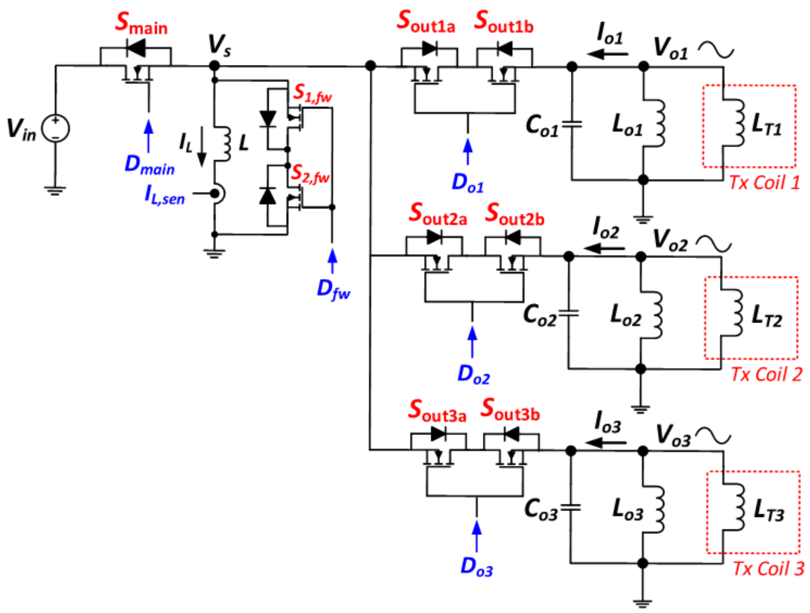


**Figure 6.** Ideal circuit diagram of buck-boost SITO inverter.

### *4.2. Operating Principle*

Figure 7a shows the switching states and operating sequence of the buck-boost SITO inverter. Figure 7b shows the theoretical waveforms of the gate-drive signals of main switch ($D_{main}$) and output switches ($D_{out1}$, $D_{out2}$, $D_{out3}$), inductor current ($I_L$), output branch currents ($I_{o1}$, $I_{o2}$, $I_{o3}$), and the three AC output voltages ($V_{o1}$, $V_{o2}$, $V_{o3}$).

For consistency, the same notation for the switching states is adopted, as explained in Section III-B. Consider the general condition of an unbalanced load, in which unequal power is delivered to the three outputs. One such example is shown in Figure 4b, where $D_{11} > D_{21} > D_{31}$. Consequently, the peak values for the inductor current $I_L$ differ for each output. Under PCCM operation, $I_L$ contains a positive DC offset, $I_{L,DC}$. Without loss of generality, the operating principle of this inverter is discussed by focusing on the first output.

In state (1-1) shown in Figure 4a, $S_{main}$ is turned ON while all other switches are turned OFF. The main inductor $L$ is charged up with $I_L$ increasing at a rate of $m_{11}$, where $m_{11} = V_{in}/L$, until it reaches a peak value ($I_{L,pk1}$) which is given by

$$I_{L,pk1} = m_{11}D_{11}T_s + I_{L,DC} = \left(\frac{V_{in}}{L}\right)D_{11}T_s + I_{L,DC} \tag{5}$$

where $D_{11}$ is the on-time duty ratio of $S_{main}$ for the first output, $T_s$ is the switching period, and $I_{L,DC}$ is the DC offset of $I_L$.

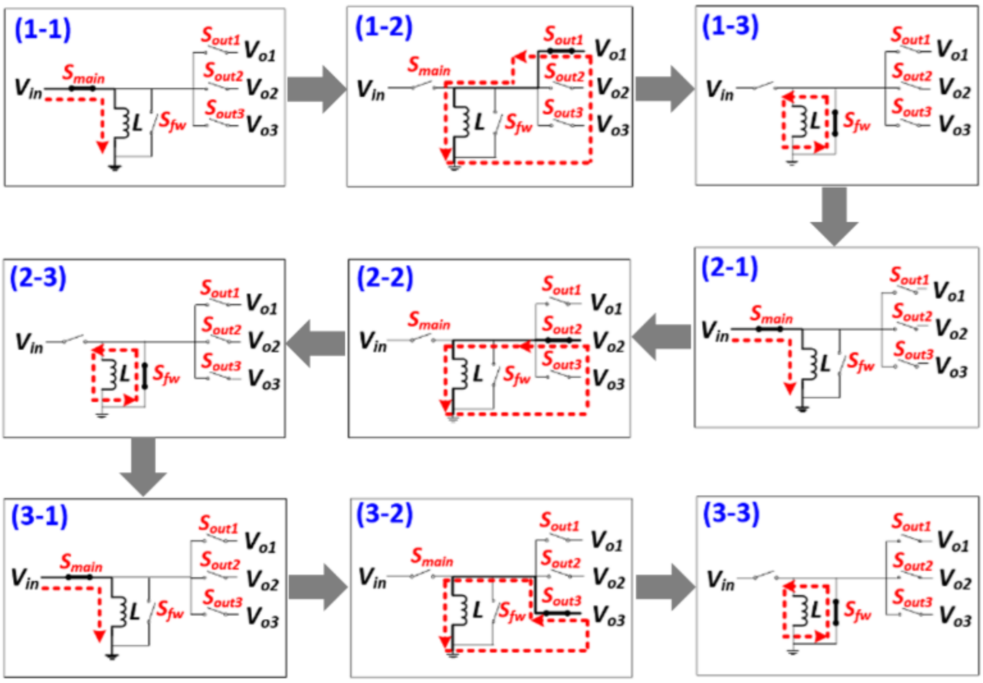


(**a**)

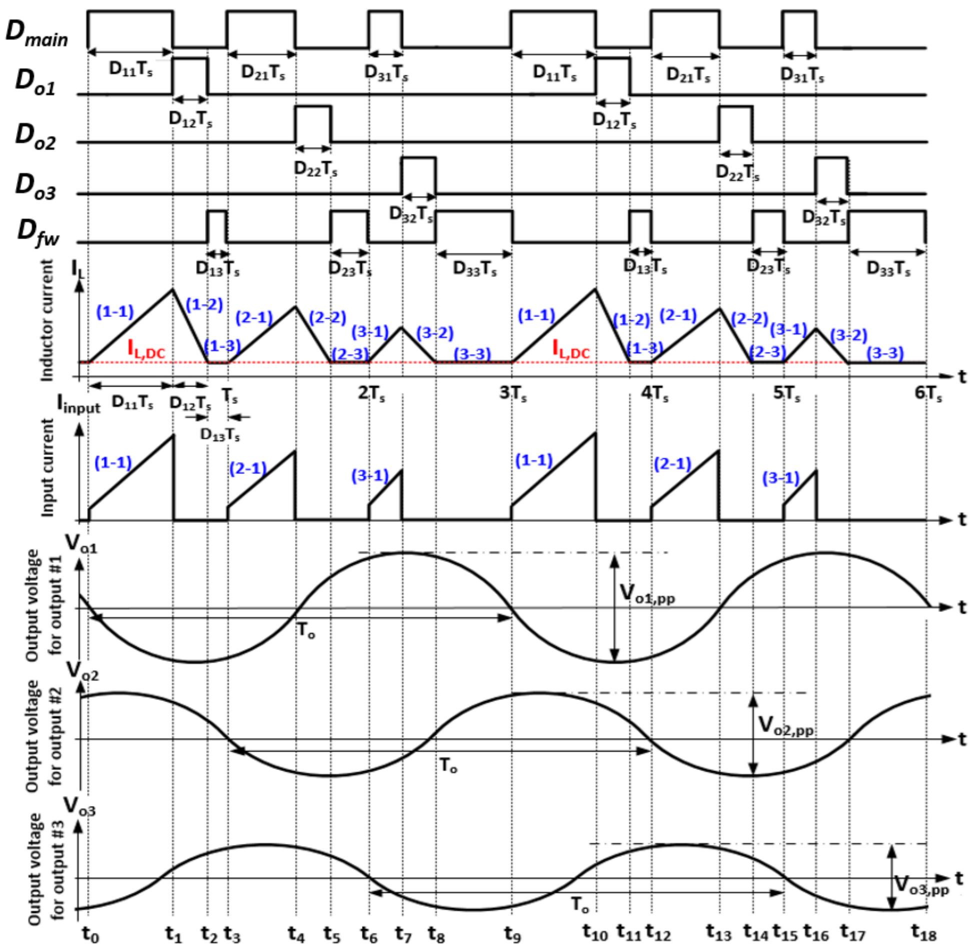


(**b**)

**Figure 7.** (**a**) Switching states and operating sequence of the buck-boost SITO inverter; (**b**) theoretical waveforms of the gate-drive signals for the main switch, output switches, main inductor current, input current, and three AC output voltages.

In state (1-2), $S_{main}$ is turned OFF, $S_{out1}$ is turned ON, while the other two output switches ($S_{out2}$, $S_{out3}$) remain OFF. During this interval, the main inductor $L$ releases its stored energy to the first output. Hence, $I_L$ decreases at a rate of $m_{12}(t)$, where $m_{12}(t) = V_{o1}(t)/L \approx V_{o1,avg}/\text{L}$, and $V_{o1,avg}$ is the average value of $V_{o1}(t)$ during state (1-2). This continues until $I_L$ reaches the valley-crossing point, i.e., $I_L = I_{L,DC}$. As shown in [8], when the duration of $D_{12}T_s$ ($D_{12}$ is the on-time duty ratio for the first output switch. It should be obvious from Figure 4b) is sufficiently short, $V_{o1,avg}$ can be approximated by the amplitude of the first output voltage $V_{m1}$. Hence, the downward slope of the inductor current ($m_{12}$) can be re-expressed as

$$m_{12} = \frac{V_{o1,avg}}{L} \approx \frac{V_{m1}}{L} \tag{6}$$

In state (1-3), only the freewheeling switches ($S_{1,fw}$, $S_{2,fw}$) are ON whereas all other switches are OFF. This creates a recycling path for the inductor current to "freewheel" between the main inductor and the freewheeling switches. In particular, in DCM operation, all switches, including the two freewheeling switches, are switched OFF. Thus, the inductor current will return to zero value in this state.

In general, for a SIMO inverter with $n$ outputs, the switching frequency ($f_s$) is $n$ times greater than the resonant frequency of the LC resonant tank ($f_o$). Mathematically, $fs$ can be expressed as

$$f_s = nf_o = \frac{n\omega_o}{2\pi} = \frac{n}{2\pi\sqrt{L_o C_o}} \tag{7}$$

## 5. Buck SIMO Hybrid Inverter

The aforementioned SIMO topologies are capable of only one type of power conversion, i.e., either DC-DC or DC-AC. This naturally raises an important question: can SIMO be designed to perform both DC-DC and DC-AC conversions simultaneously, enabling so-called hybrid conversions? Addressing this question motivates the development of a SIMO hybrid converter that can supply multiple AC and DC loads simultaneously from a single DC power source.

### *5.1. Circuit Topology*

The SIMO hybrid topology is realized through the proper integration of a DC-DC buck converter with a parallel network of LC resonant circuits and output filtering capacitors. Figure 8 graphically illustrates the derivation of the SIMO buck hybrid topology. The DC-DC stage converts the DC input voltage into a pulsating DC current. In a time-multiplexed manner, current pulses from the main inductor are directed to either the LC resonant circuit or the output filtering capacitor through the corresponding output switch. Basically, the LC resonant circuit serves as the DC-AC stage, converting the pulsating DC current into sinusoidal-like output voltages at the resonant frequency. In contrast, the output filtering capacitor suppresses high-frequency ripples, thereby producing a smooth DC output voltage. Consequently, the SIMO hybrid converter enables single-stage conversion from a DC source to either AC or DC outputs. Likewise, a boost (or buck-boost) DC-DC converter can be used to realize a SIMO boost (or buck-boost) hybrid topology.

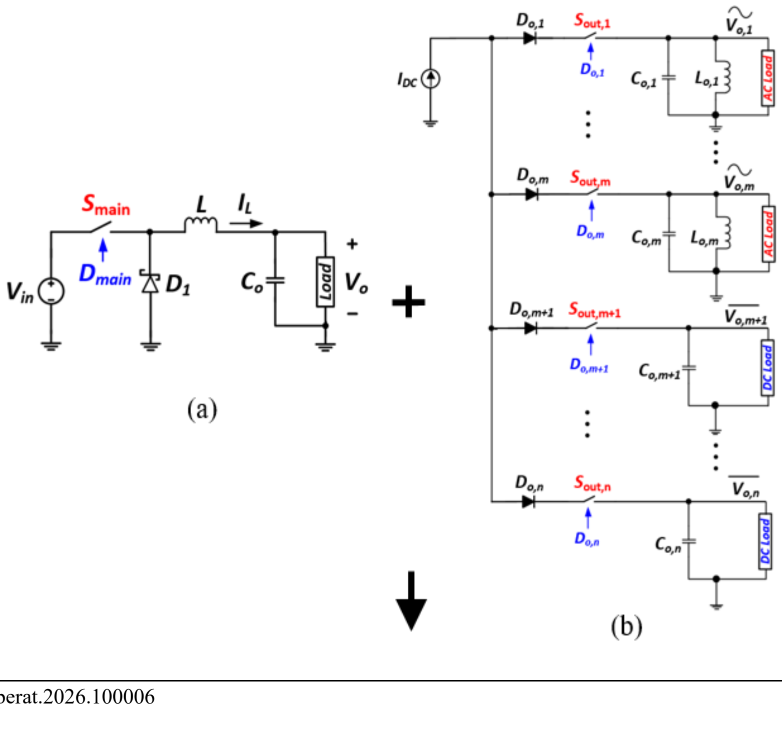


https://doi.org/10.53941/perat.2026.100006

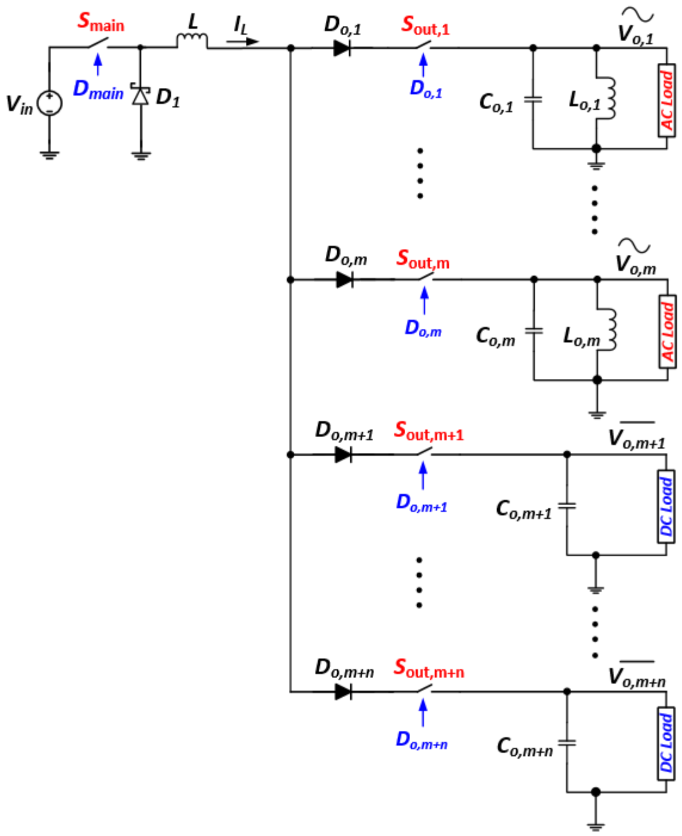


(c)

**Figure 8.** Derivation of a single-stage SIMO buck hybrid converter. (**a**) DC-DC buck converter; (**b**) ideal current source supplying a parallel network of LC resonant circuits and output filtering capacitors; and (**c**) single-stage SIMO buck hybrid converter.

The independent current source ($I_{DC}$) in Figure 8b can be replaced by the main inductor ($L$) in Figure 8a, which effectively functions as a current source. For illustration purposes, silicon power MOSFETs are employed in the SIMO hybrid converter. Accordingly, anti-series (blocking) diodes are required in each output branch to prevent undesired reverse conduction through the MOSFET body diodes. Notably, anti-series diodes are used not only in the AC output branch but also in the DC output branch to prevent potential cross-channel conduction between AC and DC output ports, as well as among the DC output ports. Alternatively, a pair of back-to-back connected silicon power MOSFETs (or even a GaN transistor) can also be used to eliminate reverse conduction.

Figure 9 shows the ideal circuit diagram of a single-inductor four-output (SIFO) buck hybrid converter with two AC outputs and two DC outputs. The SIFO converter transforms a single DC input voltage ($V_{in}$) into two sinusoidal-like AC output voltages ($V_{o1,ac}$, $V_{o2,ac}$) and two DC output voltages ($V_{o3,dc}$, $V_{o4,dc}$), albeit other combinations of AC and DC outputs are also possible. Each switch is realized as a pair of back-to-back connected power MOSFETs. The two MOSFETs are connected with their source terminals tied together, ensuring that they share the same gate-to-source voltage. This configuration also causes their intrinsic body diodes to face in opposite directions. In addition, their gate terminals are tied together, allowing both devices to be driven by a single gate driver. To illustrate the need for this arrangement, consider the case in which $Q_{m2}$ is removed, leaving only $Q_{m1}$ connected between the input voltage ($V_{in}$) and the switching node ($V_s$) in the SIFO converter. If the instantaneous value of the first AC output voltage exceeds the input voltage ($V_{o1,ac} > V_{in}$), reverse current will flow from the first output channel back to the input terminal via the body diode of $Q_{m1}$, even when $Q_{m1}$ is turned OFF and the first output is enabled. Therefore, $Q_{m2}$ is required to block this undesirable reverse current.

The output switch in each output channel is also implemented using a pair of back-to-back MOSFETs to ensure unidirectional current flow from the main inductor to the corresponding output and to eliminate cross-regulation among the outputs. For example, suppose the second MOSFET in each back-to-back pair ($Q_{o12}$, $Q_{o22}$, $Q_{o32}$, $Q_{o42}$) is removed from all output channels, and the first output channel is enabled ($Q_{o11}$ is turned ON). If the instantaneous value of the first output voltage becomes lower than that of the third output voltage ($V_{o1,ac} < V_{o3,dc}$), cross-channel current will flow from the third output channel to the first output channel through the body diode of $Q_{o31}$, even when $Q_{o31}$ is turned OFF. This results in undesirable cross-regulation between the two outputs. A similar cross-channel conduction path can also arise when two DC outputs operate at different voltage levels. Hence, the body diode of the second MOSFET in each back-to-back pair is essential for blocking unwanted conduction paths among the outputs under all operating conditions.

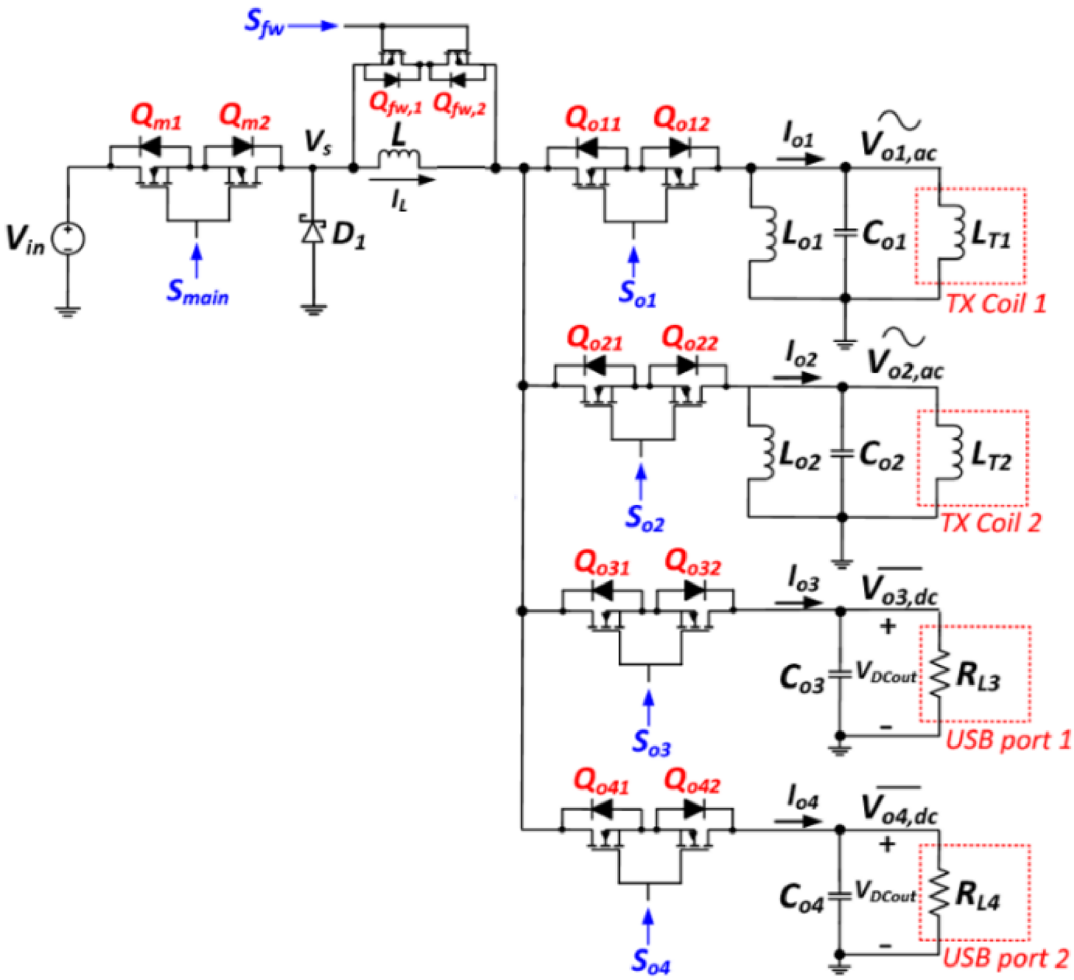


**Figure 9.** Ideal circuit diagram of SIFO buck hybrid converter.

*5.2. Operating Principle*

The SIFO hybrid converter operates in PCCM at a fixed switching frequency. Since it has four outputs, the switching frequency ($f_s$) is four times that of the resonant frequency ($f_o$), i.e., $f_s = 4f_o$. Figure 10a depicts the switching states and the corresponding equivalent circuit for each state. Since there are three distinct operating modes, the converter undergoes a total of 12 switching states. Figure 10b presents the ideal waveforms of the gate-drive signals for the main switch, output switches and freewheeling switch, alongside the inductor current and output voltages. For illustration purposes, the operating modes for DC-AC operation are discussed using the first (AC) output of the SIFO converter. Likewise, the operating modes for DC-DC operation are explained using the third (DC) output.

Consider the DC-AC operation. In state (1-1), $S_{main}$ and $S_{o1}$ are closed, while all other switches remain open. During this interval, the main inductor $L$ is energized, and the inductor current $I_L$ ramps up with a rising slope of at a rate of the inductor $m_{11}(t) = [V_{in} - V_{o1}(t)]/L$, where $V_{o1}(t) = V_{m1}\sin(\omega_o t + \phi)$, and $V_{m1}$ and $\phi$ denote the amplitude and phase angle of the sinusoidal voltage at the first output, respectively. It should be noted that the rising slope of $I_L$ is time-dependent and exhibits a concave- down characteristic; that is, the slope *decreases* as time $t$ increases over this interval. At the end of Mode 1 (e.g., $t = t_1$), $I_L$ reaches its peak value of $I_{L,pk1}$, which can be expressed as

$$I_{L,pk1} = m_{11}(t_1)D_{11}T_s + I_{L,DC} = \left[\frac{V_{in} - V_{o1}(t_1)}{L}\right]D_{11}T_s + I_{L,DC} \quad (8)$$

where $D_{11}$ is the on-time duty ratio of $S_{main}$ for the first output, and $t_1 = T_o i + D_{11}T_s = (4i + D_{11})T_s$, and $i$ is an integer.

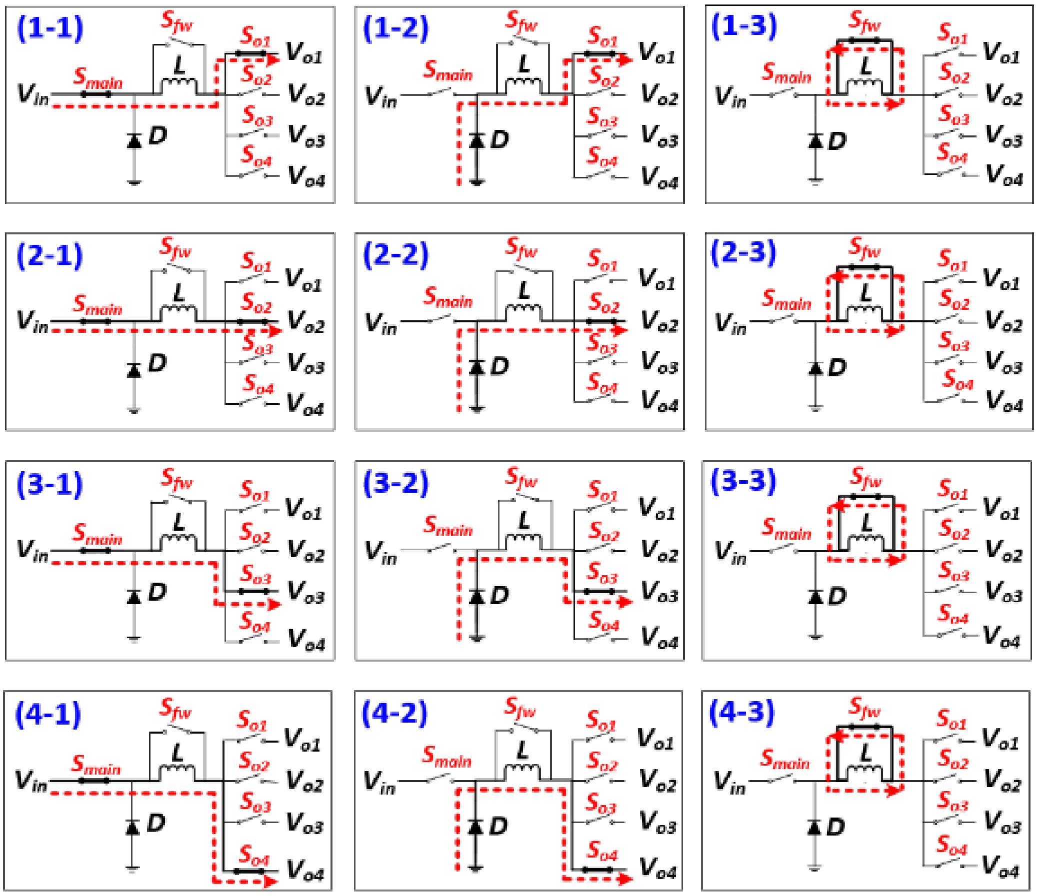


(**a**)

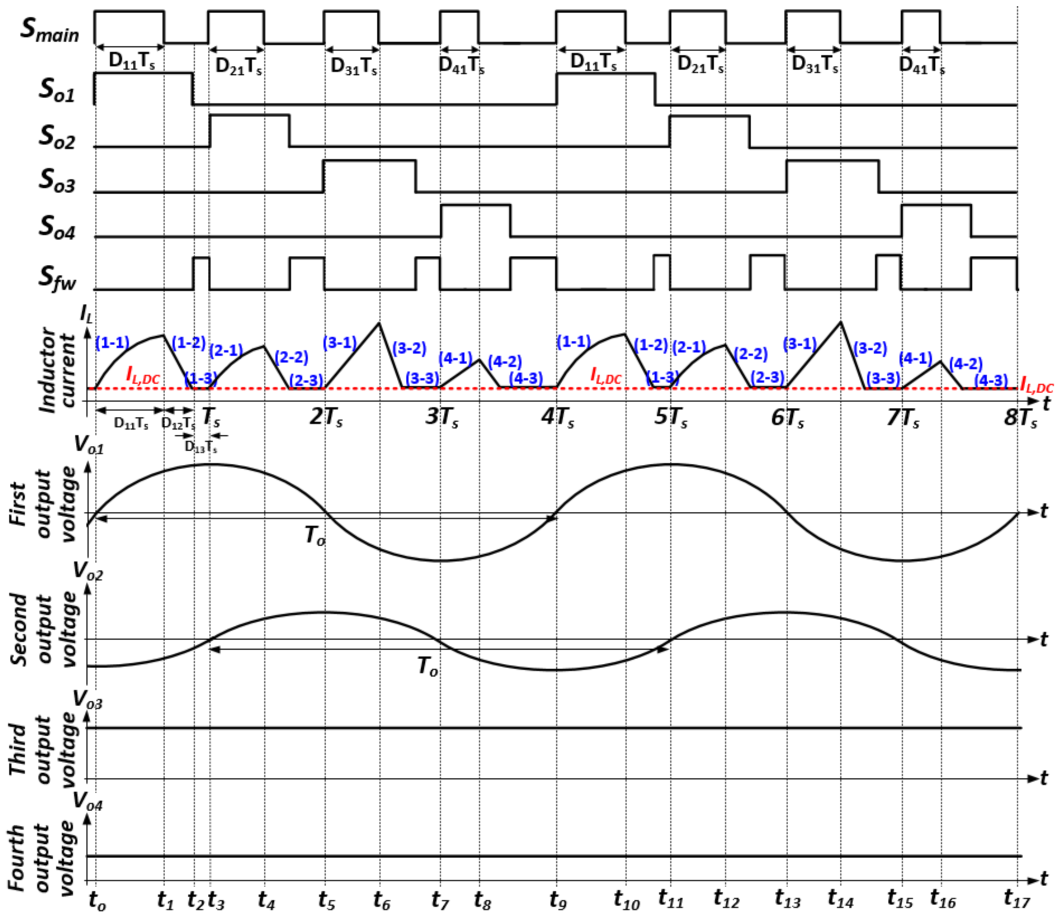


(**b**)

**Figure 10.** (**a**) Switching states; (**b**) ideal waveforms of the key signals of SIFO buck hybrid converter.

At time = $t_1$, $V_{o1}(t_1)$ can be written as

$$V_{o1}(t_1) = V_{m1}\sin(\omega_o t_1 + \phi) = V_{m1}\sin\left(\frac{\pi D_{11}}{2} + \phi\right) \tag{9}$$

The SIFO converter transitions from state (1-1) to (1-2) when $I_L$ reaches its peak value of $I_{L,pk1}$. In state (1-2), $S_{main}$ is turned OFF while $S_{o1}$ remains ON. All other output switches remain OFF. During this interval, the main inductor $L$ de-energizes into the first output, causing the inductor current $I_L$ to ramp down with a slope of $m_{12}(t) = -V_{o1}(t)/L$ until it reaches the valley-crossing point ($I_{L,DC}$). Since this interval is typically much shorter than a resonant period (i.e., $D_{12}T_s << T_o$), the variation in the sinusoidal $V_{o1}(t)$ is negligible, and thus $m_{12}(t)$ can be approximated as follows.

$$m_{12}(t) \approx m_{12} = \frac{\overline{V_{o1,m2}}}{L} \tag{10}$$

where $\overline{V_{o1,m2}}$ is the nominal value of $V_{o1}(t)$ in state (1-2).

In state (1-3), all switches, except the freewheeling switch ($S_{fw}$), are open. During this interval, $I_L$ circulates between the main inductor and the freewheeling switch of the SIFO converter.

Consider the DC-DC operation. In state (3-1), $S_{main}$ and $S_{o3}$ are turned ON while all other switches remain open. $I_L$ ramps up linearly with a rising slope of $m_{31} = [V_{in} - V_{o3}]/L$, where $V_{o3}$ is the third DC output voltage. Unlike DC-AC operation, the rising slope of $I_L$ in DC-DC operation is constant since the output voltage is DC. At the end of Mode 1 (e.g., $t = t_6$), $I_L$ eventually reaches its peak value $I_{L,pk3}$, which can be expressed as

$$I_{L,pk3} = m_{31}D_{31}T_s + I_{L,DC} = \left[\frac{V_{in} - V_{o3}}{L}\right]D_{31}T_s + I_{L,DC} \tag{11}$$

where $D_{31}$ is the on-time duty ratio of $S_{main}$ for the third output.

In state (3-2), $S_{main}$ is turned OFF and third output switch remains closed. During this interval, the main inductor releases its stored energy to the third output, and $I_L$ decreases at a rate of $m_{32} = -V_{o3}/L$ until it reaches $I_{L,DC}$. In state (3-3), all switches except the freewheeling switch are turned OFF, allowing the inductor current to freewheel. Due to the inherent time-multiplexed switching scheme in PCCM (or DCM), the operation of each output is fully decoupled in time. As a result, each output can be enabled or disabled independently without affecting the others. Standalone DC-AC operations can be readily achieved by enabling only the AC outputs while disabling the DC outputs. In this case, the SIFO converter effectively reduces to a single-inductor dual-output (SIDO) DC-AC buck inverter. Conversely, standalone DC-DC operations are realized by disabling the AC outputs and enabling only the DC outputs, in which case the SIFO converter operates as a SIDO DC-DC buck converter.

## 6. Advanced SIMO Topologies

Recent developments in SIMO-related research have expanded its scope well beyond conventional DC-DC and DC-AC applications, giving rise to a new generation of advanced topologies such as SIMO AC-AC converters and bidirectional SIMO converters. These emerging architectures are attracting increasing interest because they offer compact size, reduced component count, high scalability, and flexible power sharing among multiple loads or ports.

### *6.1. SIMO AC-AC converters*

Conventional AC-AC multiple-output power supplies require two conversion stages, namely, an AC-DC converter, followed by a parallel combination of DC-AC inverters, one per AC load. They typically require a full-bridge rectifier and a DC link capacitor to generate an intermediate pulsating voltage at double-line frequency. Such a design is bulky, costly and inefficient due to its repetitive circuit structure and excessive component count. In light of this, several single-stage SIMO AC-AC converters have been introduced in [16–18], which enable direct and efficient generation of multiple AC outputs from the AC mains supply, making them promising candidates for distributed AC power delivery and multi-load drive systems. In particular, the latest version, referred to as a non-isolated SITO AC-AC/DC hybrid converter in [19] will be discussed. Figure 11 shows the ideal circuit diagram of this hybrid converter.

Basically, the hybrid converter converts a universal AC mains supply ($V_{ac}$) into one DC output voltage ($V_{o1,dc}$) and two AC output voltages ($V_{o2,ac}$, $V_{o3,ac}$). To enable multicoil wireless power transfer, each AC output is connected to its own transmitting coil ($L_{T1}$ or $L_{T2}$), which is closely coupled to the corresponding receiving coil.

The voltage after the diode bridge ($V_s$) is a full-wave rectified sinusoidal voltage derived from $V_{ac}$. The power stage employs only a single inductor $L$, acting as a current source by transferring its stored energy to each output.

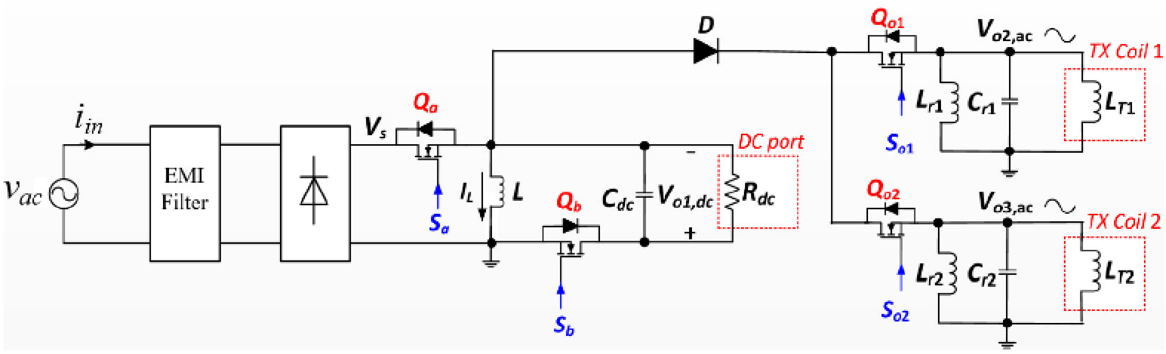


**Figure 11.** Circuit topology of SITO AC-AC/DC hybrid converter.

Similar to the SIMO inverter, each AC output branch includes a parallel LC resonant tank, which forms an integral part of the power stage. The DC output branch consists of the output capacitor ($C_{dc}$) and the resistive load ($R_{dc}$). The blocking diode ($D$) plays a crucial role by preventing undesirable reverse conduction from the AC output to the AC input or the DC output. From the perspective of the DC output, this hybrid converter behaves like an inverting buck-boost converter operating in DCM. Notably, the DC output ($V_{o1,dc}$) also serves as the input voltage for the two AC outputs, and the output power of each AC output can be independently controlled by adjusting the on-time duty ratio of $Q_b$.

Figure 12a shows the switching states and equivalent circuit for each state. Figure 12b shows the theoretical waveforms of the gate-drive signals of the four switches ($S_a$, $S_b$, $S_{o1}$, $S_{o2}$), the inductor current ($I_L$), one DC output voltage ($V_{o1,dc}$), and two AC output voltages ($V_{o2,ac}$, $V_{o3,ac}$).

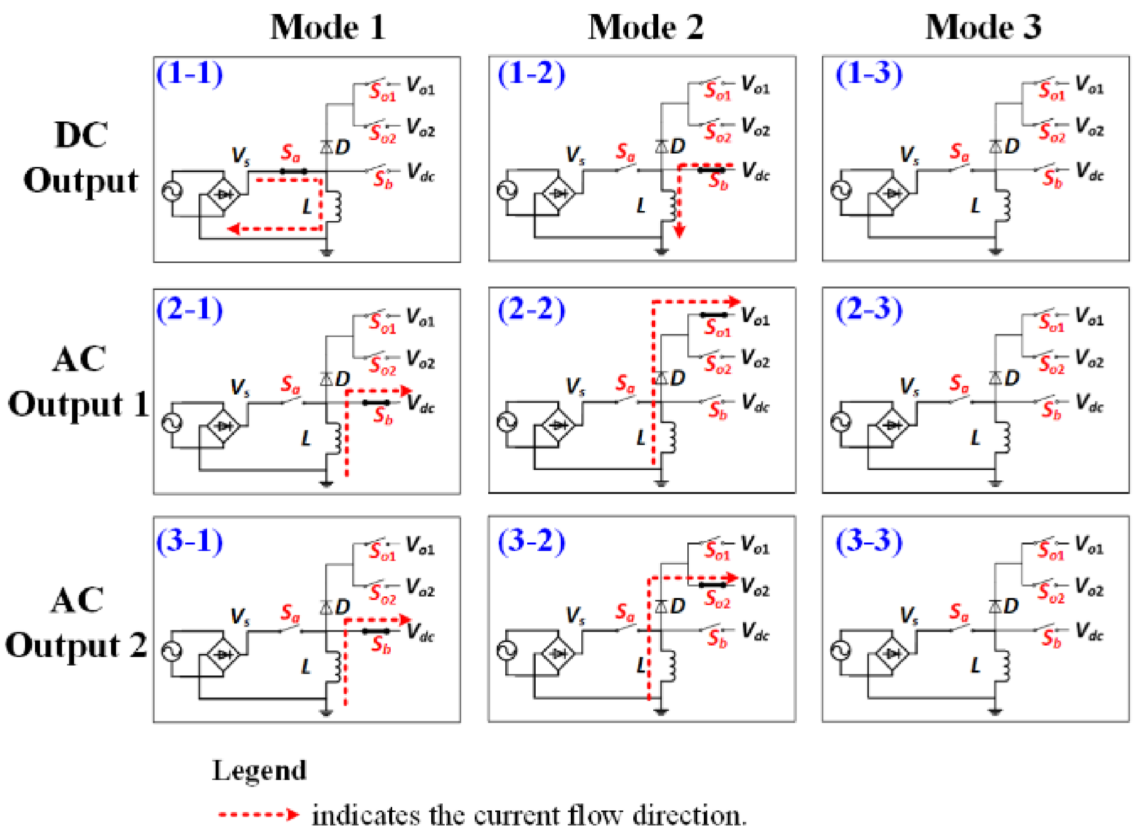


(a)

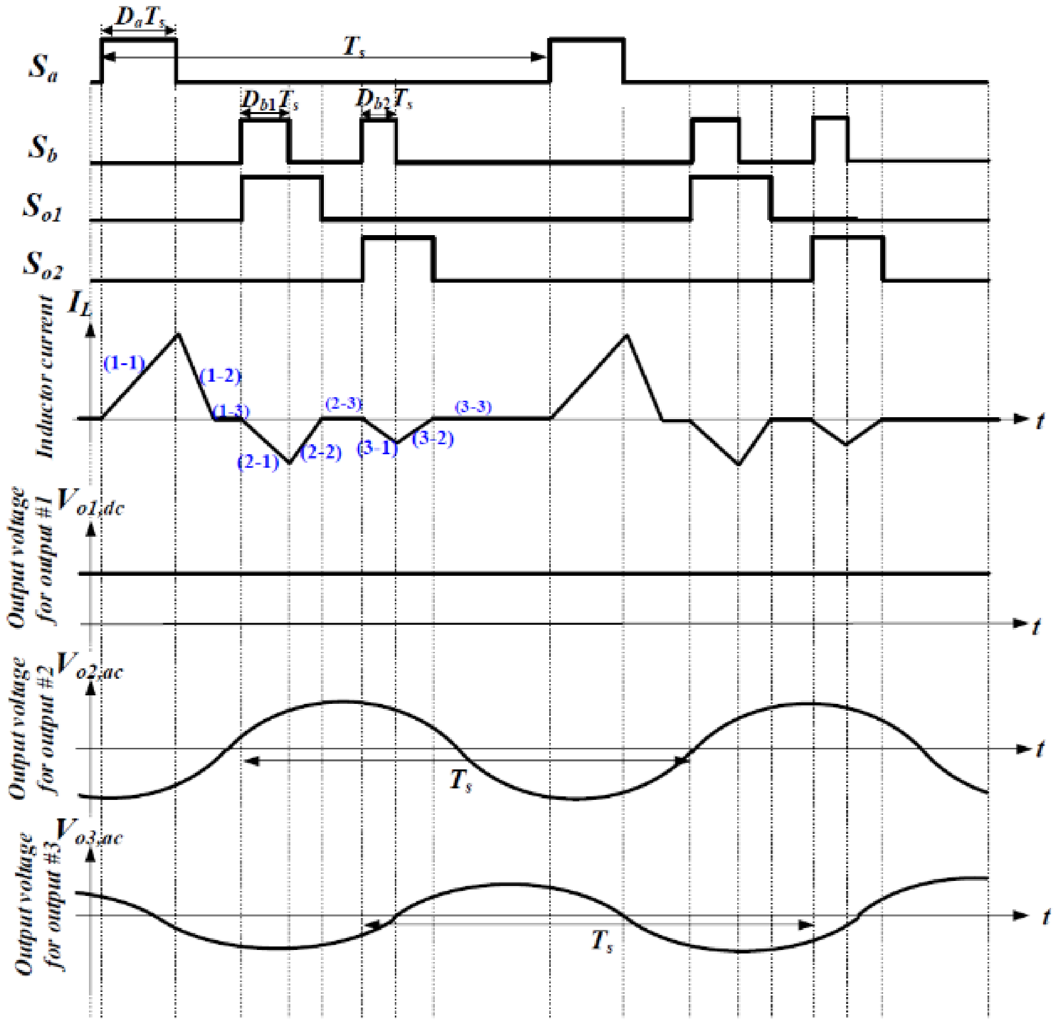


(**b**)

**Figure 12.** (**a**) Switching states and equivalent circuits of the SITO AC-AC/DC hybrid converter; (**b**) ideal waveforms of the gate-drive signals of the four switches, inductor current, and three output voltages.

A salient property of this hybrid converter is that the switching frequency is identical to the output resonant frequency. Let us consider the DC branch. In state (1-1), $S_a$ is turned ON while all other switches are OFF. The main inductor $L$ is charged up, causing $I_L$ to increase at a rate of $m_{11}$, where $m_{11} = V_s/L$. $I_L$ eventually reaches its peak value of $I_{L,pk1} = m_{11}D_aT_s$, where $D_a$ is the on-time duty ratio of $S_a$, and $T_s$ is the switching period. In state (1-2), $S_a$ is turned OFF while the body diode of $S_b$ is naturally turned ON. The main inductor discharges into the DC output, causing $I_L$ to drop at a rate of $m_{12}$, where $m_{12} = -V_{o1,dc}/L$. At the end of state (1-2), $I_L$ reaches zero value, and the body diode of $S_b$ is turned OFF. $I_L$ remains at zero in state (1-3).

Consider the AC branch. In state (2-1), only $S_b$ is turned ON while all other switches remain OFF, allowing $L$ to charge up. It should be noted that the DC output ($V_{o1,dc}$) now acts as the input power source for the AC output, which means that $I_L$ flows in the *opposite* direction and is therefore negative. $I_L$ ramps up with a slope of $m_{21}$, where $m_{21} = V_{o1,dc}/L$. At the end of (2-1), $I_L$ attains its peak value of $I_{L,pk2}$, given by $I_{L,pk2} = m_{21}D_{b1}T_s$, where $D_{b1}$ is the on-time duty ratio of $S_b$ associated with the first AC output ($V_{o2,ac}$). In state (2-2), $S_b$ is turned OFF, and $S_{o1}$ is turned ON. The main inductor discharges into the first AC output. Consequently, $I_L$ decreases with a slope of $m_{22}$, where $m_{22} = -V_{o2,ac}(t)/L$. Since the duration of state (2-2) is typically much shorter than the resonant period, the variation of $V_{o2,ac}(t)$ is small and can be approximated by its average value. Hence, $m_{22}$ may be treated as approximately constant. Finally, in state (2-3), all switches are OFF, and $I_L$ remains at zero throughout this interval. The same switching sequence is then repeated for the second AC output.

### *6.2. Bidirectional SIMO converters*

Bidirectional SIMO DC–AC converters, which enable forward (DC-AC) and reverse (AC-DC) power conversion between a single DC port and multiple AC ports, have recently been proposed in [20–23]. Figure 13 shows the circuit topology of an ideal bidirectional SIMO converter. The main module (highlighted in pink color) is derived from a modified non-inverting buck-boost converter.

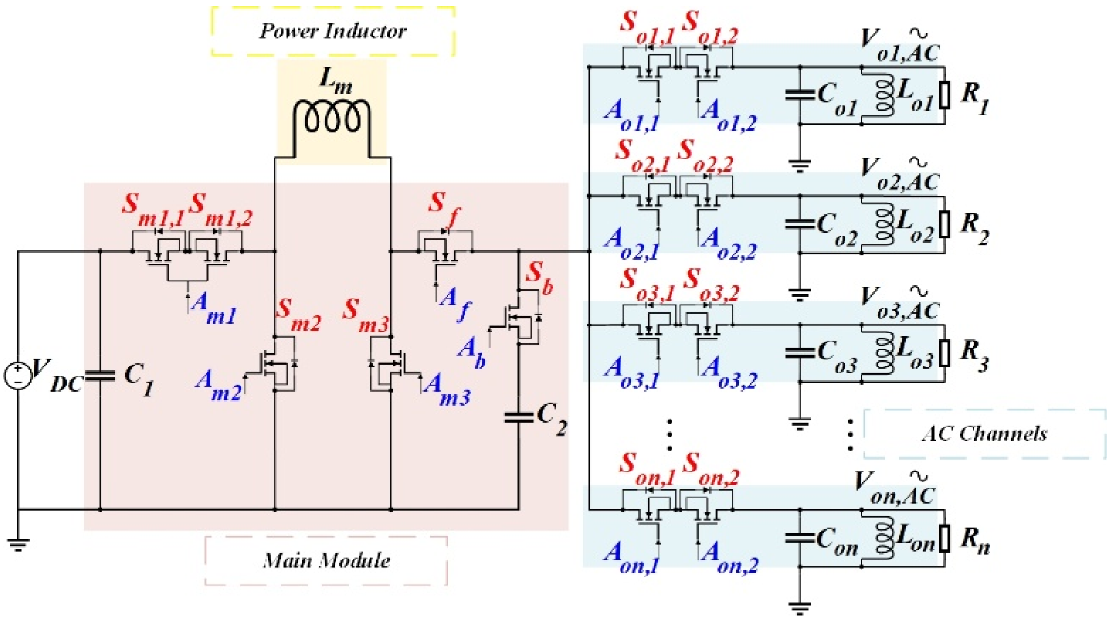


**Figure 13.** Circuit topology of an ideal bidirectional SIMO converter.

In forward DC-AC inversion, it is assumed that the first and second outputs operate in boost mode, while the third output operates in buck mode. During forward power transfer, the forward-enabling switch ($S_f$) is always turned ON whereas the backward-enabling switch ($S_b$) is always turned OFF to isolate $C_2$ from the output resonant tanks.

Figure 14a shows the switching states of the bidirectional SITO converter operating in PCCM and the corresponding equivalent circuits of each state. Figure 14b shows the ideal waveforms for the gate-drive signals for the main switches ($A_{m1}$, $A_{m2}$, $A_{m3}$) and the output switch pairs ($A_{o1}$, $A_{o2}$, $A_{o3}$), inductor current ($I_L$), and three output voltages ($V_{o1}$, $V_{o2}$, $V_{o3}$) during forward inversion.

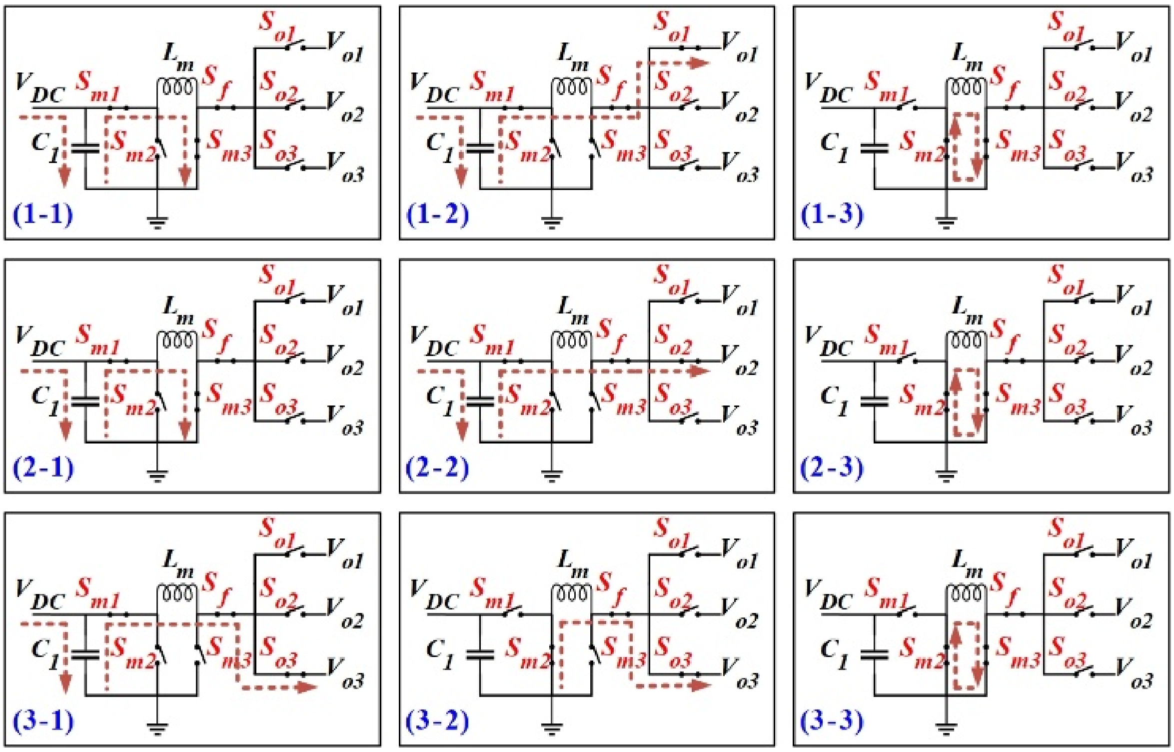


(a)

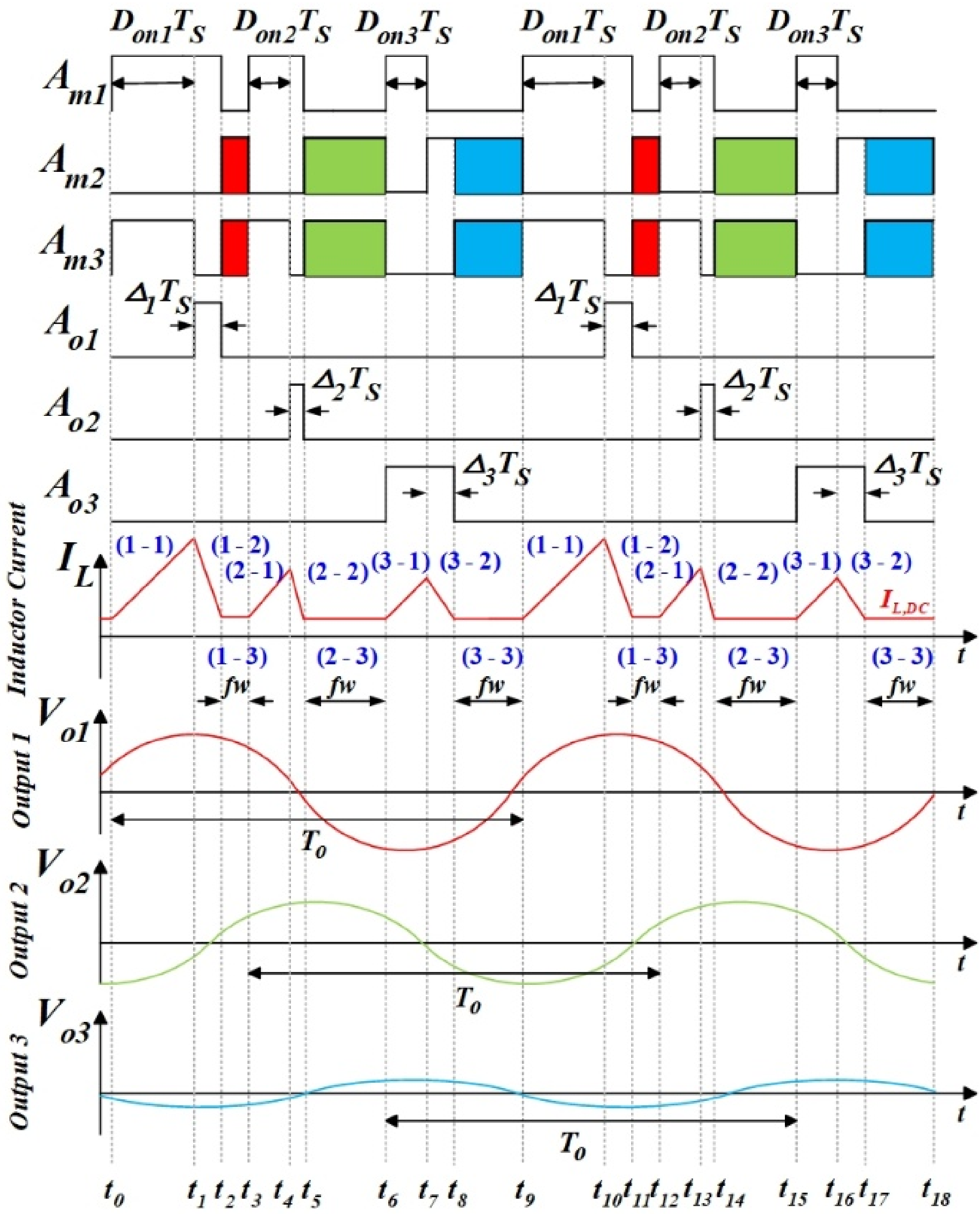


(**b**)

**Figure 14.** (**a**) Switching states and (**b**) ideal waveforms of bidirectional SITO converter in forward DC-AC inversion.

Let us consider the boost operation of the first output. In state (1-1), The main switches ($S_{m1,1}$, $S_{m1,2}$, $S_{m3}$) are turned ON, while all other switches are OFF. The main inductor ($L_M$) is charged up, and $I_L$ increases linearly with a positive slope of $m_{11} = V_{DC}/L_m$. At the end of state (1-1), $I_L$ reaches its peak value of $I_{L,pk1}$, which is given by

$$I_{L,pk1} = \frac{V_{DC}}{L_m} D_{on1} T_S + I_{L,DC} \tag{12}$$

In state (1-2), $S_{m1,1}$ and $S_{m1,2}$ remain ON, while $S_{m3}$ is turned OFF. The first output switch pairs ($S_{o1,1}$, $S_{o1,2}$) are turned ON, while all other output switches are OFF. $I_L$ then decreases at a negative rate of $m_{12} = [V_{DC} - V_{o1}(t)/L_m$. At the end of this state, $I_L$ will return to a non-zero value of $I_{L,DC}$. In state (1-3), $S_{m2}$ and $S_{m3}$ are turned ON to form a freewheeling loop for $I_L$. All other switches are in their OFF state.

In reverse AC-DC conversion, the power flow of the SITO converter is reversed. The AC ports serve as the inputs, and the DC port serves as the output. The number of active AC inputs can be arbitrary. One switch in each anti-series output pair ($S_{o1,1}$, $S_{o2,1}$, $S_{o3,1}$) is always kept OFF so that its body diodes can function as a half-wave rectifier, whereas the other switches ($S_{o1,2}$, $S_{o2,2}$, $S_{o3,2}$) are always kept ON. During reverse conversion, the backward-enabling switch ($S_b$) remains ON, allowing the filtering capacitor ($C_2$) to maintain a smooth and stable intermediate DC voltage. Owing to the symmetric structure, $S_{m1,1}$ and $S_{m1,2}$ operate as the output switches, while the forward-enabling switch ($S_f$) acts as the main switch, whose on-time duty cycle determines the value of the DC output voltage. For the sake of discussion, boost operation is assumed.

Figure 15a shows the switching states and equivalent circuits for the converter in boost PCCM operation. Figure 15b shows the ideal waveforms of the gate-drive signals for the forward-enabling switch ($A_f$) and main switches ($A_{m1}$, $A_{m2}$, $A_{m3}$), inductor current ($I_L$), and the DC output voltage ($V_{DC}$).

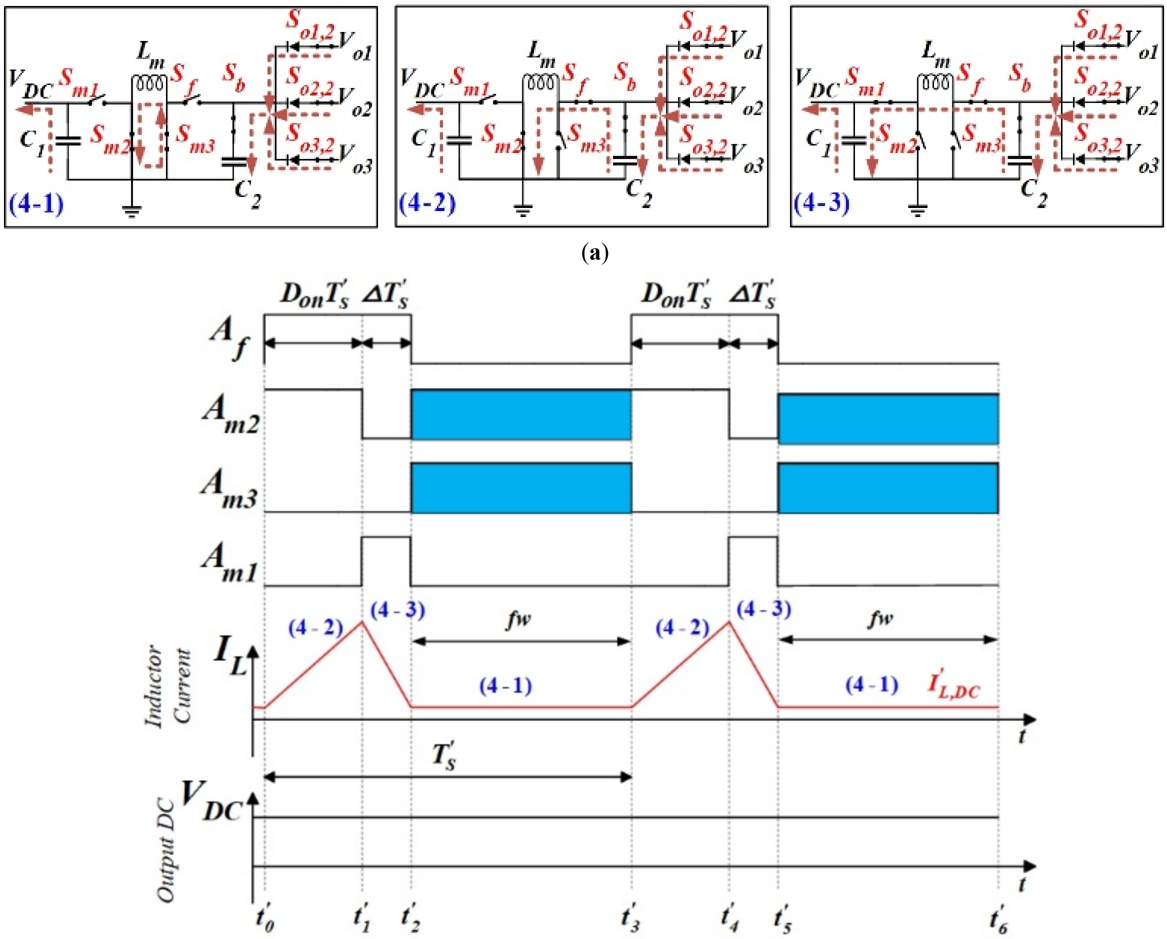


(**b**)

**Figure 15.** (**a**) Switching states and (**b**) ideal waveforms of key signals of bidirectional SITO converter in reverse AC-DC conversion.

In state (4-1), $S_b$, $S_{m2}$ and $S_{m3}$ are turned ON, while all other switches are OFF. Hence, a freewheeling path is established for the inductor current, allowing it to be maintained at a constant value of $I'_{L,DC}$. Meanwhile, the rectified AC voltage charges $C_2$, and $C_1$ continues to supply the DC output.

In state (4-2), $S_f$ is turned ON. $S_{m2}$ remains ON, and $S_{m3}$ is turned OFF. The main inductor $L_m$ is charged, and $I_L$ increases at a rate of $k_2 = V_{C2}/L_m$, where $V_{C2}$ is the voltage across $C_2$. $I_L$ attains its peak value of $I_{L,pk,PCCM}$, which can be expressed as

$$I_{L,pk,PCCM} = \frac{V_{C2}}{L_m} D_{on} T_S' + I_{L,DC}' \tag{13}$$

where $D_{ON}$ is the on-time duty-cycle of $S_f$, and $T_s'$ is the switching period.

In state (4-3), $S_f$ remains ON, and $S_{m2}$ is turned OFF. Also, $S_{m1,1}$ and $S_{m1,2}$ are turned ON, allowing $L_m$ to discharge to the DC output. $I_L$ decreases at a rate of $k_3 = (V_{C2} - V_{DC})/L_m$ until it reaches the valley-crossing point ($I'_{L,DC}$).

## 7. Design Considerations

In practice, SIMO inverters can be employed as multi-coil wireless power transmitters in multi-coil wireless power transfer (MC-WPT) systems. In such applications, the output resonant frequency of the SIMO inverter must lie within the frequency range specified by the relevant WPT standard. For instance, under the current Qi standard, power transfer is typically operated in the 110–205 kHz frequency range, with standardized power levels of up to 5 W for the Baseline Power Profile (BPP) and up to 15 W for the Extended Power Profile (EPP) or Qi2 Magnetic Power Profile (MPP). At a particular resonant frequency $f_o$, the appropriate values of $L_o$ and $C_o$ in the resonant tank can be determined as follows.

$$f_O = \frac{\omega_O}{2\pi} = \frac{1}{2\pi\sqrt{L_O C_O}} \tag{14}$$

Obviously, many combinations of $L_o$ and $C_o$ can yield the same resonant frequency. In general, it is desirable to minimize the circulating current in the LC tank at resonance in order to reduce the conduction loss caused by parasitic resistances. This can be achieved by selecting a larger $L_o$ and a smaller $C_o$, thereby increasing the overall reactance and reducing the circulating current. On the other hand, the quality factor ($Q$) of a parallel RLC circuit is given by:

$$Q = R_L \sqrt{\frac{C_O}{L_O}} \tag{15}$$

where $R_L$ denotes the equivalent output resistance. Choosing a larger $C_o$ and a smaller $L_o$ results in a higher $Q$ factor, which leads to a narrower bandwidth and greater selectivity of the resonant circuit. This is advantageous because a higher $Q$ factor suppresses harmonic components in the AC output voltage, thereby producing a cleaner, smoother sinusoidal waveform with very low distortion. It is therefore evident that, in resonant tank design, a tradeoff exists between achieving high power efficiency and minimizing total harmonic distortion. As a general rule of thumb, the reactance of $L_o$ (i.e., $X_L = \omega_o L_o$) at resonance, which is equal to the reactance of $C_o$ (i.e., $X_c = 1/\omega_o C_o$), is typically chosen to be around 2.8 Ω or so. Hence, for a given $\omega_o$, suitable values of $L_o$ and $C_o$ can be determined. For example, if the resonant frequency is 100 kHz, the values of $L_o$ and $C_o$ are about 4.5 µH and 0.56 µF, respectively.

The theoretical analysis of the SIMO inverter indicates that the AC output voltage is *not* a pure sinusoid but rather a sinusoidal-like waveform. Taking the SIMO boost inverter as an example, distortion arises in the output voltage when the inverter transitions from state (1-1) to state (1-2). This phenomenon can be explained by the difference in the fundamental frequency of the output voltage between these two states. In state (1-1), the resonant tank is completely isolated from the main inductor. As a result, the fundamental frequency of the output voltage is the same as the resonant frequency given in (14). In state (1-2), however, the main inductor ($L$) is connected to the resonant tank, which increases the fundamental frequency of the output voltage to:

$$f_1 = \frac{\omega_1}{2\pi} = \frac{1}{2\pi}\sqrt{\frac{1}{LC_O} + \frac{1}{L_O C_O}} \tag{16}$$

In theory, distortion in the output voltage can be mitigated by choosing the main inductor to be much larger than the resonant inductor (i.e., $L >> L_o$). Under this condition, the output voltage frequency becomes nearly identical to the resonant frequency in all modes of operation. However, a larger $L$ reduces the rising slope of the main inductor current ($I_L$) during state (1-1), resulting in a lower peak current. Consequently, this limits the maximum energy stored in $L$ that is subsequently be delivered to each output. This reflects a key design tradeoff between minimizing output voltage distortion and maximizing output power. From a practical standpoint, a balance must therefore be struck by choosing $L$ to be on the same order of magnitude as $L_o$, so as to provide sufficient output power while maintaining reasonably low total harmonic distortion in the output voltage. In the hardware implementation of the SIFO buck hybrid converter, $L \approx (3/4)L_o$.

Regardless of the specific SIMO topology, the dominant source of conduction loss is the equivalent-series resistance (ESR) of the main inductor ($L$). To minimize the ESR, hand-wound inductors are typically fabricated using 250 strands of 38 AWG Litz wires on an N49 core. For example, in the bidirectional SITO converter, the measured ESR of the main inductor ($L$) is as low as 15 mΩ at 300 kHz, while the resonant inductor exhibits an ESR of approximately 12.9 mΩ at 100 kHz. In addition, the on-resistance ($R_{dsON}$) of the power MOSFETs also contributes to the overall conduction loss. In particular, during reverse power conversion in a bidirectional SIMO converter, the conduction loss associated with the body diodes of the output MOSFETs must also be taken into account. On the other hand, the parasitic capacitances of MOSFETs are the dominant source of switching loss. Replacing silicon power MOSFETs with GaN transistors can help reduce switching loss because GaN devices typically exhibit lower gate charge, lower output capacitance, and negligible reverse-recovery charge. These characteristics enable faster switching transitions and reduce the overlap between voltage and current during turn-on and turn-off, making GaN particularly attractive for high-frequency power conversion.

## 8. Conclusions

SIMO inverters, SIMO hybrid converters, SIMO AC-AC converters and bidirectional SIMO converters offer a compact and efficient solution for multiport power conversion by employing a shared inductor to reduce component count, system size, and implementation cost. SIMO inverters are well suited for generating multiple AC outputs from a single source. SIMO AC-AC converters enable direct AC power conversion with relatively simple circuit configurations, while bidirectional SIMO converters further extend operation capability by enabling reversible power flow. Notwithstanding these merits, several challenges such as cross-regulation, control complexity, dynamic response and loss minimization remain critical to practical implementation. Yet, ongoing advances in modulation and control techniques, magnetic component design, soft-switching strategies and wide-bandgap semiconductor devices are expected to further improve the performance and applicability of SIMO converter topologies in high-power-density and multifunctional power electronic systems.

## 9. Biographies of the authors

**Albert Ting Leung Lee** received the B.Sc. (Distinction) degree in electrical engineering from the University of Wisconsin, Madison, WI, USA, in 1994, the M.Sc. degree in electrical and computer engineering from the University of Michigan, Ann Arbor, MI, USA, in 1996, and the Ph.D. degree in electronic and computer engineering with The Hong Kong University of Science and Technology, Hong Kong, China, in 2014. He is currently a Senior Lecturer with the Department of Electrical and Computer Engineering, The University of Hong Kong, Hong Kong. His research interests include power electronics and control, LED lightings, wireless power transfer, and generative AI. He is a Member of HKIE.

**Siew-Chong Tan** received the B.Eng. (Hons.) and M.Eng. degrees in electrical and computer engineering from the National University of Singapore, Singapore, in 2000 and 2002, respectively, and the Ph.D. degree in electronic and information engineering from the Hong Kong Polytechnic University, Hong Kong, in 2005. He is currently a Chair Professor in Department of Electrical Engineering, City University of Hong Kong, Hong Kong. Previously, he held academic positions at the University of Hong Kong and Hong Kong Polytechnic University. He has also held visiting appointments at the Grainger Center for Electric Machinery and Electromechanics, University of Illinois at Urbana–Champaign, USA; Nanyang Technological University, Singapore; and Huazhong University of Science and Technology, Wuhan, China. His research interests are focused in the areas of power electronics and control, LED lightings, smart grids, and clean energy technologies. He is Fellow of IEEE and HKIE.

## Author Contributions

In this paper, A.T.L.L. made the primary intellectual and writing contribution by drafting the manuscript and developing the paper's written content in full. This included organizing the technical discussion, presenting the core ideas clearly, and shaping the overall narrative of the study so that the design concepts and application aspects of SIMO inverters were communicated in a coherent and accessible manner. S.-C.T. contributed in an advisory and editorial role, providing guidance on the scope of the paper and its overall organization to ensure that the manuscript remains focused, well-structured, and aligned with its intended academic objectives. In addition, the second author carefully proofread the manuscript, helping to improve its clarity, consistency and presentation quality prior to submission. Both authors have read and agreed to the published version of the manuscript.

## Funding

This research was funded by Prof. Tan’s CityU startup funding project number 9380174.

## Institutional Review Board Statement

Not applicable.

## Informed Consent Statement

Not applicable.

## Data Availability Statement

Not applicable.

## Conflicts of Interest

The authors declare no conflict of interest.

## Use of AI and AI-Assisted Technologies

No AI tools were utilized for this paper.

## References

1. Ma, D.; Ki, W.H.; Mok, P.K.T.; et al. Single-Inductor Multiple-Output Switching Converters with Bipolar Outputs. In Proceedings of the 2001 IEEE International Symposium on Circuits and Systems (Cat. No.01CH37196), Sydney, NSW, Australia, 6–9 May 2001; pp. 301–304.
2. Ma, D.; Ki, W.H.; Tsui, C.Y.; et al. A 1.8 V Single-Inductor Dual-Output Switching Converter for Power Reduction Techniques. In Proceedings of the 2001 Symposium on VLSI Circuits. Digest of Technical Papers (IEEE Cat. No.01CH37185), Kyoto, Japan, 14–16 June 2001; pp. 137–140.
3. Ki, W.H.; Ma, D. Single-Inductor Multiple-Output Switching Converters. In Proceedings of the 2001 IEEE 32nd Annual Power Electronics Specialists Conference (IEEE Cat. No.01CH37230), Vancouver, BC, Canada, 17–21 June 2001; pp. 226–231.
4. Ma, D.; Ki, W.H.; Tsui, C.Y.; et al. Single-Inductor Multiple-Output Switching Converters with Time Multiplexing Control in Discontinuous Conduction Mode. *IEEE J. Solid-State Circuits* **2003**, *38*, 89–100. https://doi.org/10.1109/jssc.2002.806279.
5. Ma, D.; Ki, W.H.; Tsui, C.Y. A Pseudo-CCM/DCM SIMO Switching Converter with Freewheel Switching. *IEEE J. Solid-State Circuits* **2003**, *38*, 1007–1014. https://doi.org/10.1109/jssc.2003.811976.
6. Bonizzoni, E.; Borghetti, F.; Malcovati, P.; et al. A 200 mA 93% Peak Efficiency Single-Inductor Dual-Output DC-DC Buck Converter. In Proceedings of the 2007 IEEE International Solid-State Circuits Conference, San Francisco, CA, USA, 11–15 February 2007; pp. 526–619. https://doi.org/10.1109/isscc.2007.373526.
7. Ma, D.; Ki, W.H.; Tsui, C.Y.; et al. Single-Inductor Multiple-Output Switching Converters in PCCM with Freewheel Switching. US7432614B2, 7 October 2008.
8. Huang, M.H.; Chen, K.H. Single-Inductor Multi-Output (SIMO) DC-DC Converters with High Light-Load Efficiency and Minimized Cross-Regulation for Portable Devices. *IEEE J. Solid-State Circuits* **2009**, *44*, 1099–1111. https://doi.org/10.1109/jssc.2009.2014726.
9. Leng, C.W.; Yang, C.H.; Tsai, C.H. Digital PWM Controller for SIDO Switching Converter with Time-Multiplexing Scheme. In Proceedings of the 2009 International Symposium on VLSI Design, Automation and Test (VLSI-DAT), Hsinchu, Taiwan, 28–30 April 2009; pp. 52–55. https://doi.org/10.1109/vdat.2009.5158093.
10. Kwon, D.; Rincon-Mora, G.A. Single-Inductor-Multiple-Output Switching DC-DC Converters. *IEEE Trans. Circuits Syst. II Express Briefs* **2009**, *56*, 614–618. https://doi.org/10.1109/tcsii.2009.2025629.
11. Eachempatti, H.; Ganta, S.; Silva-Martinez, J.; et al. SIDO Buck Converter with Independent Outputs. In Proceedings of the 53rd IEEE International Midwest Symposium on Circuits and Systems, Seattle, WA, USA, 1–4 August 2010; pp. 37–40. https://doi.org/10.1109/mwscas.2010.5548555.
12. Jing, X.; Mok, P.K.T.; Lee, M.C. A Wide-Load-Range Constant-Charge Auto-Hopping Control Single-Inductor-Dual-Output Boost Regulator with Minimized Cross-Regulation. *IEEE J. Solid-State Circuits* **2011**, *46*, 2350–2362. https://doi.org/10.1109/jssc.2011.2162188.
13. Chen, H.; Zhang, Y.; Ma, D. A SIMO Parallel-String Driver IC for Dimmable LED Backlighting with Local Bus Voltage Optimization and Single Time-Shared Regulation Loop. *IEEE Trans. Power Electron.* **2012**, *27*, 452–462. https://doi.org/10.1109/tpel.2011.2160404.
14. Moon, Y.J.; Roh, Y.S.; Gong, J.C.; et al. Load-Independent Current Control Technique of a Single-Inductor Multiple-Output Switching DC-DC Converter. *IEEE Trans. Circuits Syst. II Express Briefs* **2012**, *59*, 50–54. https://doi.org/10.1109/tcsii.2011.2173969.
15. Lee, A.T.L.; Sin, J.K.O.; Chan, P.C.H. Scalability of Quasi-Hysteretic FSM-Based Digitally Controlled Single-Inductor Dual-String Buck LED Driver to Multiple Strings. *IEEE Trans. Power Electron.* **2014**, *29*, 501–513. https://doi.org/10.1109/tpel.2013.2253804.
16. Jin, W.; Lee, A.T.L.; Li, S.; et al. Low-Power Multichannel Wireless Transmitter. *IEEE Trans. Power Electron.* **2018**, *33*, 5016–5028. https://doi.org/10.1109/tpel.2017.2730482.

17. Lee, A.T.L.; Jin, W.; Li, S.; et al. Single-Stage Single-Inductor Multiple-Output (SIMO) Inverter Topology with Precise and Independent Amplitude Control for Each AC Output. US10903756B2, 26 January 2021.
18. Lee, A.T.L.; Jin, W.; Tan, S.C.; et al. Buck-Boost Single-Inductor Multiple-Output High-Frequency Inverters for Medium-Power Wireless Power Transfer. *IEEE Trans. Power Electron.* **2019**, *34*, 3457–3473. https://doi.org/10.1109/tpel.2018.2855678.
19. Lee, A.T.L.; Jin, W.; Tan, S.C.; et al. Single-Inductor Multiple-Output (SIMO) Buck Hybrid Converter for Simultaneous Wireless and Wired Power Transfer. *IEEE J. Emerg. Sel. Top. Power Electron.* **2022**, *10*, 2163–2177. https://doi.org/10.1109/jestpe.2020.3002987.
20. Ray, O.; Mishra, S. Boost-Derived Hybrid Converter with Simultaneous DC and AC Outputs. *IEEE Trans. Ind. Appl.* **2014**, *50*, 1082–1093. https://doi.org/10.1109/tia.2013.2271874.
21. Adda, R.; Ray, O.; Mishra, S.K.; et al. Synchronous Reference-Frame-Based Control of Switched Boost Inverter for Standalone DC Nanogrid Applications. *IEEE Trans. Power Electron.* **2013**, *28*, 1219–1233. https://doi.org/10.1109/tpel.2012.2211039.
22. Vakacharla, V.R.; Chauhan, A.K.; Reza, M.M.; et al. Boost Derived Hybrid Converter: Problem Analysis and Solution. In Proceedings of the 2016 IEEE International Conference on Power Electronics, Drives and Energy Systems (PEDES), Trivandrum, India, 14–17 December 2016; pp. 1–5. https://doi.org/10.1109/pedes.2016.7914332.
23. Chauhan, A.K.; Kumar, R.R.; Raghuram, M.; et al. Extended Buck-Boost Derived Hybrid Converter. In Proceedings of the 2017 IEEE Industry Applications Society Annual Meeting, Cincinnati, OH, USA, 1–5 October 2017; pp. 1–8. https://doi.org/10.1109/ias.2017.8101766.
24. Chauhan, A.K.; Vakacharla, V.R.; Reza, M.M.; et al. Modified Boost Derived Hybrid Converter: Redemption Using FCM. *IEEE Trans. Ind. Appl.* **2017**, *53*, 5893–5904. https://doi.org/10.1109/tia.2017.2721921.
25. Ahmad, A.; Bussa, V.K.; Singh, R.K.; et al. Quadratic Boost Derived Hybrid Multi-Output Converter. *IET Power Electron.* **2017**, *10*, 2042–2054. https://doi.org/10.1049/iet-pel.2017.0171.
26. Wu, J.; Lee, A.T.L.; Tan, S.C.; et al. A Direct AC-AC Single-Inductor Multiple-Output (SIMO) Converter for Multi-Coil Wireless Power Transfer Applications. In Proceedings of the IEEE Energy Conversion Congress and Exposition (ECCE), Detroit, MI, USA, 11–15 October 2020; pp. 5495–5500. https://doi.org/10.1109/ecce44975.2020.9235667.
27. Wu, J.; Lee, A.T.L.; Tan, S.C.; et al. Bridgeless Single-Stage Single-Inductor Multiple-Output (SIMO) AC-AC Converter Topology. US11489452B2, 1 November 2022.
28. Wu, J.; Lee, A.T.L.; Tan, S.C.; et al. A Bridgeless Single-Stage Single-Inductor Multiple-Output (SIMO) AC-AC Converter for Wireless Power Transfer Applications. In Proceedings of the 2023 IEEE Wireless Power Technology Conference and Expo, San Diego, CA, USA, 4–8 June 2023.
29. Wu, J.; Lee, A.T.L.; Tan, S.C.; et al. Non-Isolated Buck-Boost Hybrid Converter with AC-AC/DC Power Conversion for Simultaneous Wired and Wireless Power Transfer. In Proceedings of the 2022 IEEE Applied Power Electronics Conference and Exposition (APEC), Houston, TX, USA, 20–24 March 2022; pp. 1863–1869. https://doi.org/10.1109/apec43599.2022.9773428.
30. Ji, C.; Lee, A.T.L.; Wu, J.; et al. A Bidirectional Single-Inductor Multiple-Output (SIMO) Buck-Boost Converter for Multi-Coil Wireless Power Transfer Applications. In Proceedings of the IEEE Energy Conversion Congress and Exposition, Phoenix, AZ, USA, 20–24 October 2024; pp. 3253–3258.
31. Ji, C.; Lee, A.T.L.; Wu, J.; et al. Isolated Bidirectional Single-Input Multiple-Output Converter for Peer-to-Peer Wireless Power Transfer. In Proceedings of the 2025 IEEE Wireless Power Technology Conference and Expo (WPTCE), Rome, Italy, 3–6 June 2025.
32. Ji, C.; Lee, A.T.L.; Wu, J.; et al. A New Bidirectional Single-Inductor Multiple-Output (SIMO) DC-AC Converter for Low-Power Applications. *IEEE Trans. Ind. Electron.* **2025**, *72*, 12126–12137. https://doi.org/10.1109/tie.2025.3582581.
33. Ji, C.; Wu, J.; Lee, A.T.L.; et al. Design Optimization of a Bidirectional Single-Inductor Multiple-Output (SIMO) DC-AC Converter. In Proceedings of the IEEE Applied Power Electronics Conference and Exposition (APEC), San Antonio, TX, USA, 22–26 March 2026; pp. 596–601. https://doi.org/10.1109/apec51134.2026.11516724.
34. Galizzi, M.; Caldara, M.; Re, V.; et al. A Novel Qi-Standard Compliant Full-Bridge Wireless Power Charger for Low Power Devices. In Proceedings of the 2013 IEEE Wireless Power Transfer Conference (WPTC), Perugia, Italy, 15–16 May 2013; pp. 44–47. https://doi.org/10.1109/wpt.2013.6556877.
35. Pantic, Z.; Lee, K.; Lukic, S.M. Multifrequency Inductive Power Transfer. *IEEE Trans. Power Electron.* **2014**, *29*, 5995–6005. https://doi.org/10.1109/tpel.2014.2298213.
36. Ahn, D.; Mercier, P.P. Wireless Power Transfer with Concurrent 200-kHz and 6.78-MHz Operation in a Single-Transmitter Device. *IEEE Trans. Power Electron.* **2016**, *31*, 5018–5029. https://doi.org/10.1109/tpel.2015.2480122.
37. Zhao, C.; Costinett, D. GaN-Based Dual-Mode Wireless Power Transfer Using Multifrequency Programmed Pulse Width Modulation. *IEEE Trans. Ind. Electron.* **2017**, *64*, 9165–9176. https://doi.org/10.1109/tie.2017.2681974.
38. Li, H.; Wang, K.; Fang, J.; et al. Pulse Density Modulated ZVS Full-Bridge Converters for Wireless Power Transfer Systems. *IEEE Trans. Power Electron.* **2019**, *34*, 369–377. https://doi.org/10.1109/tpel.2018.2812213.